	$Z+$ 1 jet	$Z+$ 2 jets	$Z+ \geq 3$ jets
CDF lepton and vertex tag background expectation	17.5	4.2	1.5
CDF lepton and vertex tag data	15	3	2
DO muon tag background expectation	0.97 ± 0.08	0.35 ± 0.05	0.09 ± 0.03
D0 muon tag data	0	0	0

TABLE XIII. Comparison between the number of observed tags in $Z+$ jets data and the background expectations. The CDF results are from Gerdes, 1995, and correspond to an integrated luminosity of 67 pb^{-1}. The D0 results are from Abachi *et al.*, 1995d, and are based on the Run Ia data set only, with an integrated luminosity of 13.5 pb^{-1}.

an order of magnitude lower than the cross-section for $p\bar{p} \rightarrow W \rightarrow l\nu$, giving only limited statistics in the Z channel. Nevertheless, it is still instructive to compare the yield of tags in the Z sample with the results of the background calculations. This is especially true in light of the fact that two out of the three $Z+ \geq 3$ jets events collected by CDF during run Ia contained one vertex-tagged jet (F. Abe *et al.*, 1994a).

The results of the tagging algorithms on $Z+$ jets events are displayed in Table XIII. With the higher luminosity data sample, the number of tags in the $Z+$ jets data is fully consistent with the background expectations, within the limited statistics. There is no evidence for an anomalously high tagging rate in Z events.

To summarize, the CDF and D0 background calculations have been proved to be reliable and, within the statistical and systematic uncertainties, they have been shown to be able to account for the rate of tagged jets in both $Z+$ jets and $W+$ 1 and 2 jets. There is significant evidence for the presence of an excess of b-jets in the $W+ \geq 3$ jets sample. The largest excess is seen in the CDF vertex tag analysis, which has the highest efficiency and the best signal-to-background. The statistical significances of these excesses, which are consistent in size with the expected $t\bar{t}$ contribution, will be discussed in Section VIII.D.

It is very natural to attribute these excesses to a $t\bar{t}$ component in the data, although they could also be due to some source of $W+$ heavy flavor production beyond standard QCD processes. As we will show in Section VIII.C, additional evidence for the existence of the top quark can be obtained by kinematic studies of lepton + jets events. Furthermore, studies of invariant masses in lepton + jets events show evidence for both $t \rightarrow Wb; W \rightarrow l\nu$ and $t \rightarrow Wb; W \rightarrow q\bar{q}$, see Section IX.

	Leptons		Jets				
Channel	$E_T(e)$	$P_T(\mu)$	$N_{\rm jet}$	E_T	$\not{E}_T$	H_T	$\mathcal{A}$
$e+$jets	≥ 20		≥ 4	≥ 15	≥ 25	≥ 200	≥ 0.05
$\mu+$jets		≥ 15	≥ 4	≥ 15	≥ 20	≥ 200	≥ 0.05

TABLE XIV. D0 kinematic requirements for the standard event selection (energies in GeV, momenta in GeV/c). From Abachi *et al.*, 1995b.

C. Lepton + jets

Both CDF and D0 have performed analyses based on event shapes or kinematic variables rather than b-quark identification in order to increase their $t\bar{t}$ acceptance. They have both used some form of a powerful discriminator between $W+$ jets background and top signal, which is the scalar sum of the transverse energies of the jets and in some cases leptons. D0 has performed an analysis on a data set complementary to the lepton + jet + b-tag data set. That is, it starts with the sample of lepton + jet events in which a b-tag is not found. The results from this counting experiment are used in calculating the significance of the top signal. CDF on the other hand, performs two separate kinematic analyses on the complete lepton+jet data sample which includes b-tagged events. These analyses are however not used in calculating the significance of the top signal both because their results are correlated with the b-tag result, and because kinematic analyses depend to a greater extent on Monte Carlo generation details and theoretical assumptions.

In comparing the data with the theoretical expectations for $W+$ jets, the CDF and D0 analyses use the VECBOS Monte Carlo. As discussed in Section V.E.1, VECBOS is a leading order QCD parton Monte Carlo. Models of the underlying event and of jet fragmentations have been added to VECBOS by both collaborations to allow for comparisons with experimental data.

1. D0 lepton + jet kinematic analysis

The requirements for this analysis are given in Table XIV. This analysis requires that there be at least four jets in the event, in contrast to the b-tag analysis which includes events with three jets. The two main kinematic requirements are that the scalar sum of the transverse energies of the jets, H_T, be >200 GeV and that the event be aplanar such that, $\mathcal{A}$ >0.05. Aplanarity, $\mathcal{A}$, was defined in Section V.E.3 as $\mathcal{A}\equiv 3/2\lambda_1$, where λ_1 is the smallest eigenvalue of the matrix $M_{ab}=\sum P_a P_b/\sum P^2$, where P_i are the cartesian components of momentum of the parton, P is the magnitude of the three-momentum, and the sum is over all partons. In the D0 analysis, $\mathcal{A}$ is calculated from the jets in the event. Note that the definition of H_T in the D0 lepton + jets analysis is different than the definition of H_T in the dilepton analysis, where the E_T of the highest transverse energy electron was also included, see Section VIII.A. Fig. 82 shows the distribution H_T for top quarks produced by Monte Carlo and expectations for principal backgrounds. There is expected to be a clear separation between signal and background.

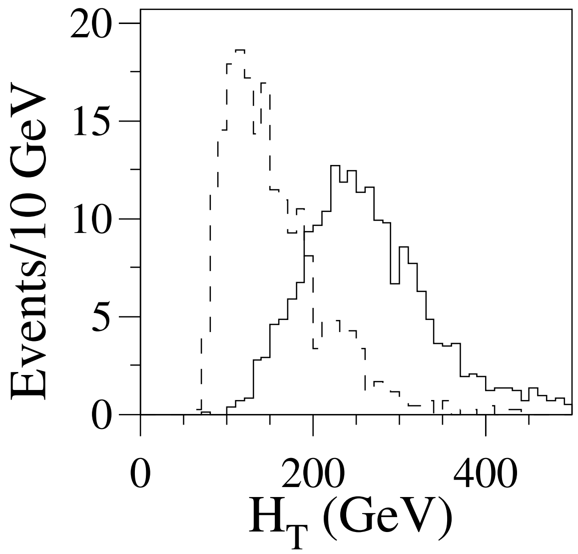

FIG. 82. Expected H_T distributions in D0 for top Monte Carlo events with M_{top} = 200 GeV/c^2 in the lepton + jets + no b-tag sample (solid) and the principal backgrounds to this channel (dashed). From Abachi *et al.*, 1995b.

This analysis must rely on the correctness of both the Monte Carlo kinematics and the energy scale of the calorimeters. To check the combined effect, comparisons are performed between data and Monte Carlo distributions of H_T for two samples dominated by background, $W+ \geq 2$ jets and $W+ \geq 3$ jets. Fig. 83 shows the data and VECBOS Monte Carlo prediction for these two samples. These samples may contain some top events, but are dominated by $W+$ jets background if the theoretical expectations for the $t\bar{t}$ production cross-section are correct. The agreement between the data and the Monte Carlo prediction is quite good.

The acceptance, including branching ratio (24/81, see Table III), for the D0 $t\bar{t}$ kinematic search ranges from 0.50% for M_{top} = 140 GeV/c^2 to 1.70% for M_{top} = 200 GeV/c^2. The expected background, the expected signal and the data are shown in Table XV, and Fig. 84.

The two main sources of background in this analysis are QCD events in which one jet fakes the lepton signature and, especially, $W+ \geq 4$ jet events. The QCD background is calculated by studying a sample of events containing electromagnetic clusters that fail the lepton selection requirements. The estimation of the $W+$ jets background is clearly a crucial issue. This background is estimated in two ways (Abachi *et al.*, 1995d; Grannis, 1995). In the first method, the number of $W+ \geq 4$ jets events in the data is estimated by extrapolating from the number of $W+ \geq 2$ and 3 jets events assuming a scaling law, i.e. assuming that the ratio N_n/N_{n-1} is independent of n, where N_n is the number of QCD $W+ \geq n$ jets events, (see Fig. 85 and Fig. 86). Then, the number of $W+ \geq 4$ jets events expected to satisfy the aplanarity and H_T requirement is obtained from N_4 and the shape of the VECBOS Monte Carlo distribution for $W+ \geq 4$ jets in the $\mathcal{A}$ vs. H_T plane, (see Fig. 84). An alternative estimate is obtained by fitting the number of events in the four regions of the $\mathcal{A}$ vs. H_T plane indicated in Fig. 84 to contributions from $t\bar{t}$, $W+ \geq 4$ jets and QCD events, where the shapes of the $t\bar{t}$ and $W+ \geq 4$ jets components are taken from Monte Carlo. The two methods are in reasonable agreement. The total expected background is 1.9 ± 0.5 events

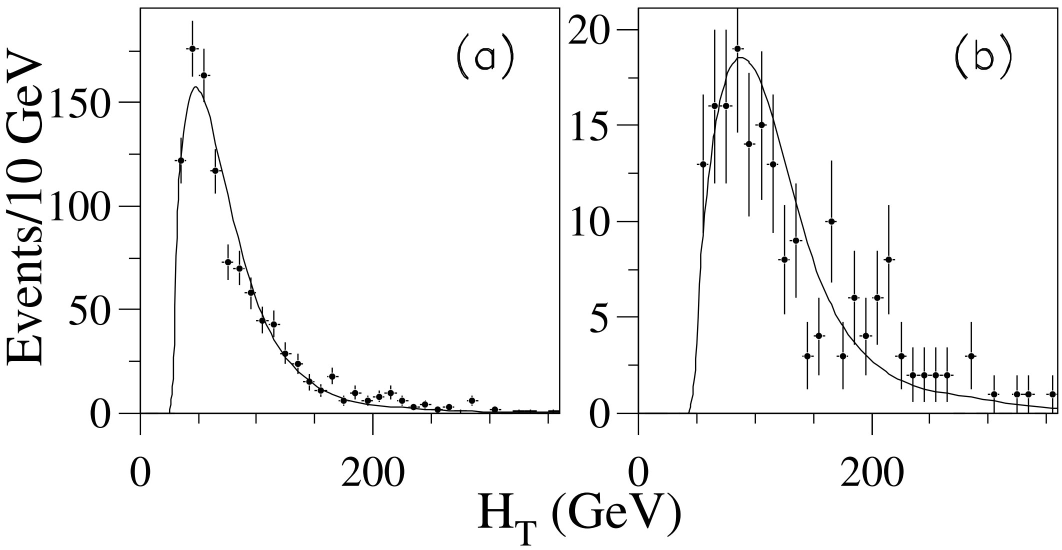

FIG. 83. D0 H_T distributions for (a) e + $\geq$ 2 jets, and (b) e + $\geq$ 3 jets The curves are expectations from the VECBOS Monte Carlo normalized to the data. From Snyder, 1995a, for an integrated luminosity of 48 pb^{-1}.

for the scaling method, and $2.6^{+0.5}_{-0.8} \pm 0.5$ events for the fit in the $\mathcal{A}$ vs. H_T plane (Grannis, 1995).

		Events
e + jets	Expected background	1.22 ± 0.42
	Expected for M_{top} = 140 GeV/c^2	4.05 ± 0.94
	Expected for M_{top} = 200 GeV/c^2	1.8 ± 0.31
	D0 data	5
μ + jets	Expected backgrounds	0.71 ± 0.28
	Expected for M_{top} = 140 GeV/c^2	2.47 ± 0.68
	Expected for M_{top} = 200 GeV/c^2	0.95 ± 0.24
	D0 data	3

TABLE XV. D0 Lepton + jets results. From Abachi *et al.*, 1995b. The integrated luminosities are 48 pb^{-1} for e + jets and 44 pb^{-1} for μ+ jets. The $t\bar{t}$ expectations are normalized to the $\sigma(t\bar{t})$ calculation of Laenen, Smith, and van Neerven, 1994.

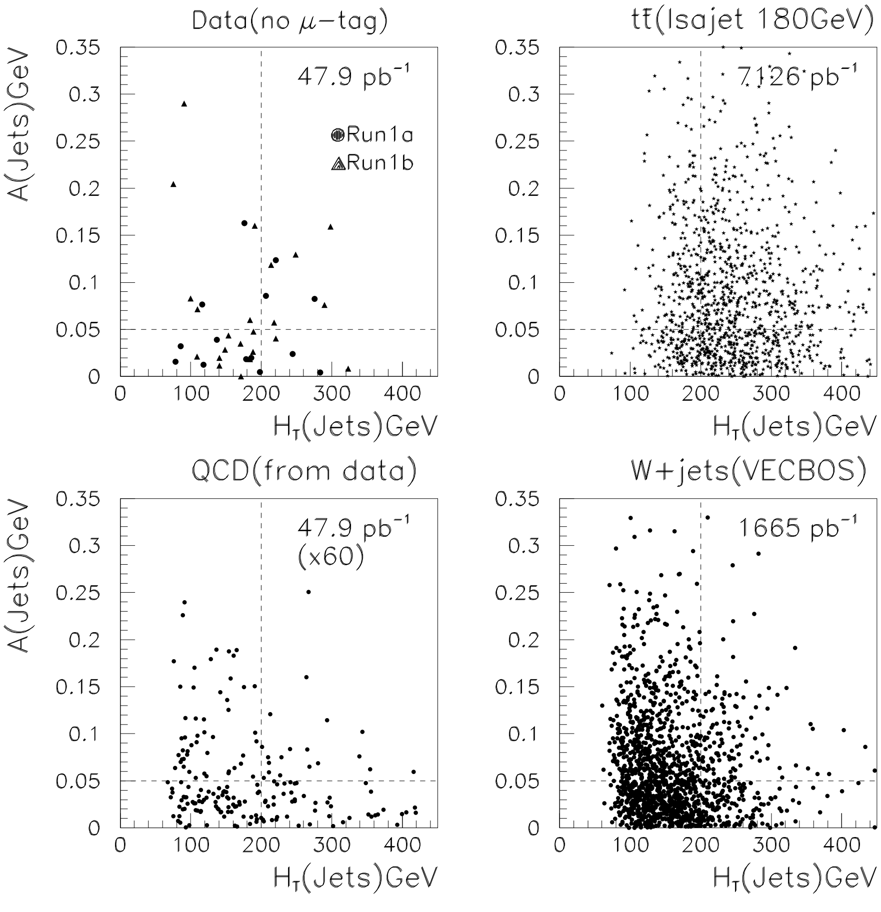

FIG. 84. Aplanarity ($\mathcal{A}$) versus H_T for single-lepton events for data, $t\bar{t}$ Monte Carlo, multijet background from data (with an effective luminosity = 60 x data luminosity), and background from $W+$ jets VECBOS Monte Carlo. From the D0 collaboration, Abachi *et al.*, 1995f.

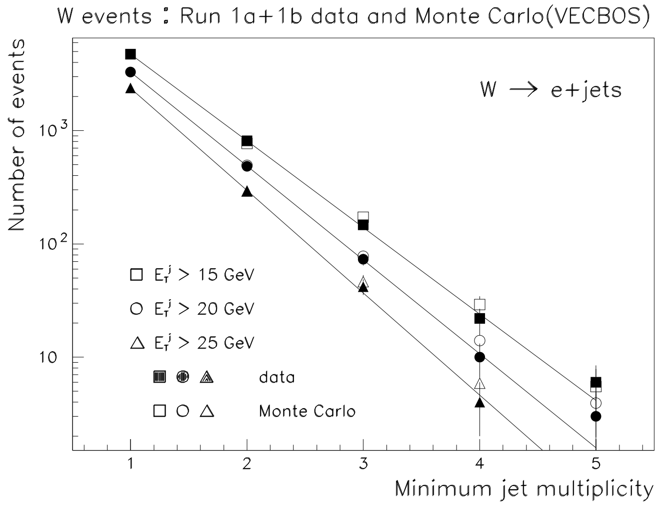

FIG. 85. Inclusive jet multiplicity spectrum for $W \to e\nu$ + jets events for several jet energy thresholds. Data are shown by the solid symbols. Monte Carlo predictions are shown by the open symbols. From the D0 collaboration, Abachi *et al.*, 1995f. The integrated luminosity is 48 pb^{-1}.

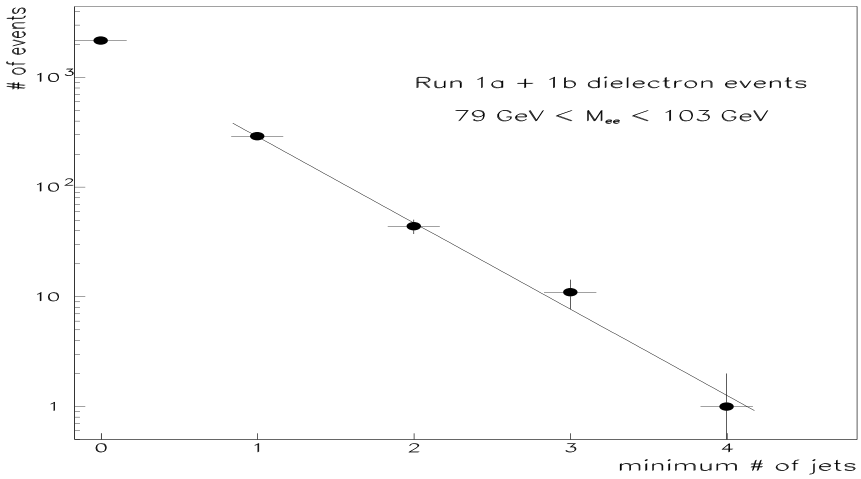

FIG. 86. Inclusive jet multiplicity spectrum for $Z \to ee+$ jets events. From the D0 collaboration, Snyder, 1995a. The integrated luminosity is 56 pb^{-1}.

Sample	Threshold	N_{jets}	E_T (GeV)	$\|\eta_{jet}\|$	Events
Control	low	=3	≥ 8	≤ 2.4	814
		Veto jet 4	≥ 8	≤ 2.4	
Control	high	=3	≥ 15	≤ 2.0	104
		Veto jet 4	≥ 8	≤ 2.4	
Signal	low	≥ 4	≥ 8	≤ 2.4	267
Signal	high	≥ 3	≥ 15	≤ 2.0	99
		≥ 1	≥ 8	≤ 2.4	

TABLE XVI. CDF definition of the two control and two signal samples in the H analysis. The third, fourth and fifth columns list the criteria placed on the jets in each event. The integrated luminosity is 67 pb^{-1}.

2. CDF lepton + jets kinematic analysis

Two kinematic analyses of lepton + jets data have been published by the CDF collaboration. The first analysis (*H analysis*, F. Abe *et al.*, 1995c) is similar to the D0 analysis. The second analysis (*cosθ^* analysis*, F. Abe *et al.*, 1995b) relies on the fact that jets in $t\bar{t}$ events are more central than jets in $W+$ jets.

The variable H in CDF is defined as the scalar sum of the lepton transverse momentum, the $\not{E}_T$ (i.e. the P_T of the ν) and the E_T's of all jets with $E_T \geq 8$ Gev and pseudo-rapidity $|\eta| \leq 2.4$. Note that while the event selection uses uncorrected jet transverse energies, H is calculated using corrected energies. The difference between the variables H used by CDF and H_T used by D0 is the inclusion of the measurements of $\not{E}_T$ and lepton momentum in H.

The H analysis is performed by comparing the observed H distribution in the data with prediction from the $W+$ jets and $t\bar{t}$ Monte Carlos. A deviation from the $W+$ jets expectation would then signal the presence of $t\bar{t}$ in the data. Note that this approach is totally independent of theoretical expectations for the $W+$ jets cross-section since it relies only on the predicted shape of the H distribution. In order to check the reliability of the theoretical prediction, the data H distribution is compared with theoretical predictions in four different samples, two control samples and two signal samples, see Table XVI.

The two control samples reject events with a fourth jet. These samples are designed to be dominated by background, and are a good testing ground for the VECBOS $W+$ jets calculation. There are less than 10 $t\bar{t}$ expected in each sample. The first control sample has a low requirement on the transverse energy of the jets, to further increase the proportion of $W+$ jet background relative to top events. The two signal samples require the presence of a fourth jet. The first signal sample is obtained with a low transverse energy threshold on the jets (8 GeV); in the second signal samples, which is expected to be enriched in $t\bar{t}$ events, at least three of the four jets must have transverse energies greater than 15 GeV.

Data-Monte Carlo comparisons for the control samples and the signal samples are displayed in Fig. 87 and Fig. 88. The shape of the H distribution in the control samples agrees with the $W+$ jets VECBOS Monte Carlo, while the two signal samples are not consistent

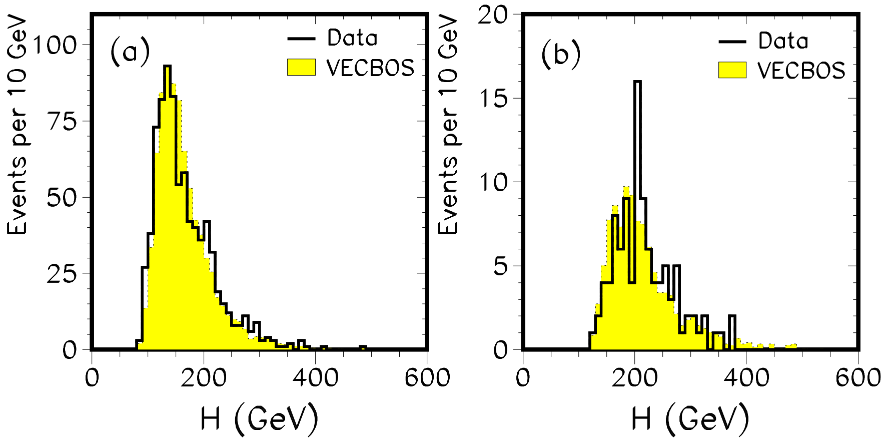

FIG. 87. Comparison of the H distribution for the control data samples and the VECBOS Monte Carlo prediction. (a) $W+3$ jets events passing the low E_T threshold requirements; (b) $W+3$ jets events passing the high E_T threshold requirements. The VECBOS prediction, including a 1% $t\bar{t}$ contribution for (a) and 10% $t\bar{t}$ contribution for (b), has been normalized to the data. From the CDF collaboration, F. Abe *et al.*, 1995c. The integrated luminosity is 67 pb^{-1}.

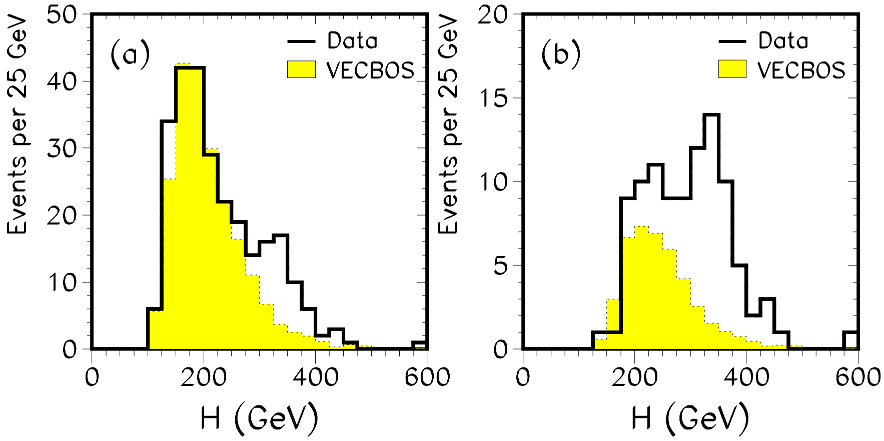

FIG. 88. Comparison of the H distribution for the signal data samples and the VECBOS Monte Carlo prediction. (a) $W+\geq 4$ jets events passing the low E_T threshold requirements; (b) $W+\geq 4$ jets events passing the high E_T threshold requirements. The VECBOS prediction is normalized to a fit to the sum of $t\bar{t}$ and $W+4$ jets Monte Carlo predictions. From the CDF collaboration, F. Abe *et al.*, 1995c. The integrated luminosity is 67 pb^{-1}.

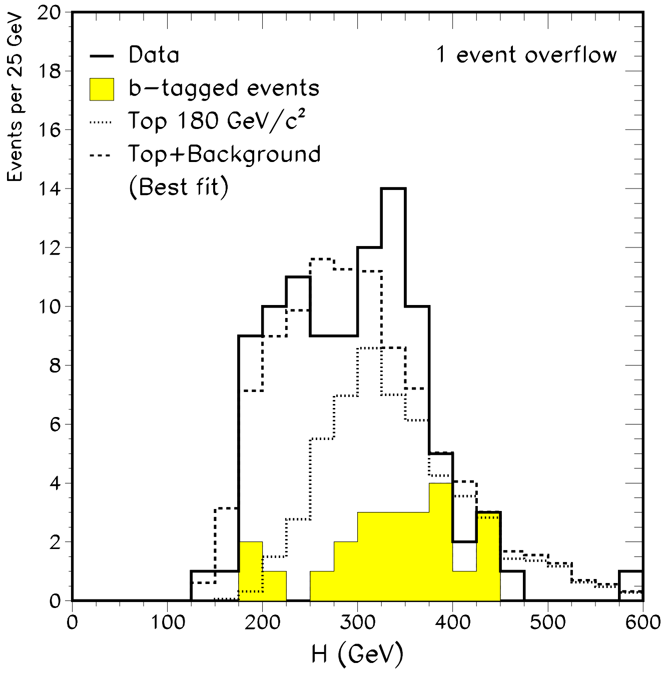

FIG. 89. The binned likelihood fit of the high E_T threshold signal sample (solid line) to a linear combination of the VECBOS $W+4$ jets and HERWIG $t\bar{t}$ Monte Carlo prediction. The H distribution of b-tagged events is shown in the shaded histogram. From the CDF collaboration, F. Abe *et al.*, 1995c. The integrated luminosity is 67 pb^{-1}.

with $W+$ jets production alone. The differences between the high threshold signal sample and the VECBOS Monte Carlo is too large to be explained entirely by a systematic error in the experimental energy scale.

The shape of the H distribution for $t\bar{t}$ events is expected to be a function of M_{top}. Fitting the data to a linear combination of $W+$ 4 jets and $t\bar{t}$ Monte Carlo prediction yields $M_{top} = 180 \pm 12(\text{stat.})^{+19}_{-15}(\text{syst.})$ GeV/c^2. This value for M_{top} is in good agreement with both the expected value from the Standard Model and with the directly measured value, see Section IX. Furthermore, the $t\bar{t}$ cross-section extracted from this measurement is also in good agreement with the cross-section extracted from studies of dilepton and b-tagged events, see Section VIII.E.

As a further evidence for $t\bar{t}$, the events containing b-tags are highlighted in Fig. 89. These events are concentrated at high values of H, as would be expected for $t\bar{t}$. Note that in background events there is a small dependence on the b-tag probability as a function of jet E_T, and hence as a function of H, which biases the tagged events to high H. However, if one assumes that there are no $t\bar{t}$ events in the sample, this bias is not sufficient to account for the concentration of tagged events at high values of H.

The second CDF kinematic analysis of lepton + jets data, (cosθ^* analysis, F. Abe *et al.*, 1995b), is based on the fact that jets in top events are expected to be more central than in $W+$ jets events (Cobal, Grassman, and Leone, 1994). This analysis is also based on control and signal samples, see Table XVII. The only difference in the two samples is in the requirement on the cosine of the polar angle (θ^*) of the jets in the center of mass frame

Channel	Leptons E_T(e)	$P_T(\mu)$	Jets $N_{\rm jet}$	E_T	$\lvert\cos\theta^*\rvert$	$\not{E}_T$	$l\nu$ transverse mass
Signal $e+$jets	≥ 20		≥ 3	≥ 20	≤ 0.7	≥ 25	≥ 40
Signal $\mu+$jets		≥ 20	≥ 3	≥ 20	≤ 0.7	≥ 25	≥ 40
Control $e+$jets	≥ 20		≥ 3	≥ 20	≥ 0.7	≥ 25	≥ 40
Control $\mu+$jets		≥ 20	≥ 3	≥ 20	≥ 0.7	≥ 25	≥ 40

TABLE XVII. CDF kinematic requirements for the $\cos\theta^*$ kinematic analysis. $\cos\theta^*$ is the cosine of the polar angle of the jet in the center of mass frame of the lepton + neutrino + jets system. The $\cos\theta^*$ requirement applies to the three highest E_T jets only. Unlike all other CDF analyses, in this analysis jet energies are corrected at the event selection stage. Energies are in GeV, momenta are in GeV/c. From F. Abe *et al.*, 1995b. The integrated luminosity is 67 pb^{-1}.

of the two incoming partons. Events in the signal sample have three high E_T central jets, events in the control sample have at least one jet that is emitted in the forward or backward region. Monte Carlo studies indicate that top events should be approximately equally split between signal and control samples, whereas of order 75% of $W+$ jets events should be in the control sample. Thus, the signal sample should be enriched in top quarks with respect to the control sample.

An event-by-event Monte Carlo-based relative likelihood for the $t\bar{t}$ versus the $W+$ jets hypothesis is constructed for all events based on the E_T of the second and third highest E_T jets in the event. Distributions of log-likelihood for data and Monte Carlo, for both signal and control sample, are displayed in Fig. 90 and Fig. 91. There is a clear excess of events at high log-likelihood in the signal sample. The probability that the shape of the data log-likelihood distribution can be explained by $W+$ jets alone is $< 0.26\%$, assuming the VECBOS model of $W+$ jets production. Furthermore, the b-tagged events are concentrated in the high log-likelihood region, as one would expect for $t\bar{t}$.

3. Summary of lepton + jets kinematic analyses

The CDF and D0 collaborations have performed extensive studies of the kinematic properties of lepton + jet events. The $W+$ jets data are inconsistent with the expectations from leading order QCD as implemented in the VECBOS Monte Carlo program, for high jet multiplicities and high jet transverse energies. On the other hand, there seems to be satisfactory agreement between data and theory in regions of low jet multiplicity and/or low jet transverse energies. The conclusion that can be drawn is that either the available QCD calculation is incorrect or incomplete, or that there is a source of events beyond standard QCD production of $W+$ jets. The most natural interpretation of the data is to ascribe this discrepancy to a $t\bar{t}$ component in the data. The correlation between high jet transverse energies and b-tags reported by the CDF collaboration strengthens this conclusion.

As was mentioned in Section V.E.3, samples of $Z+$ jets events are ideal to test the predictive power of the vector-boson + jets QCD calculation. A number of such tests have been performed, and they seem to yield results consistent with the QCD calculation. However, the statistics in the Z samples are not sufficient to decisively validate the QCD

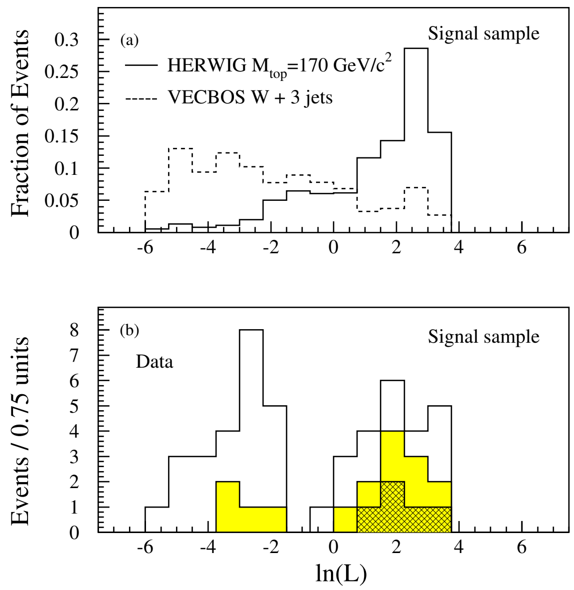

FIG. 90. The distribution in natural log-likelihood for events in the signal sample. (a) Monte Carlo expectations for $W+$ jets (VECBOS) and $t\bar{t}$ (HERWIG); (b) Data. The lightly shaded histogram shows the b-tagged events. The darkly shaded histogram shows events with two b-tags. From the CDF collaboration, F. Abe *et al.*, 1995b. The integrated luminosity is 67 pb^{-1}.

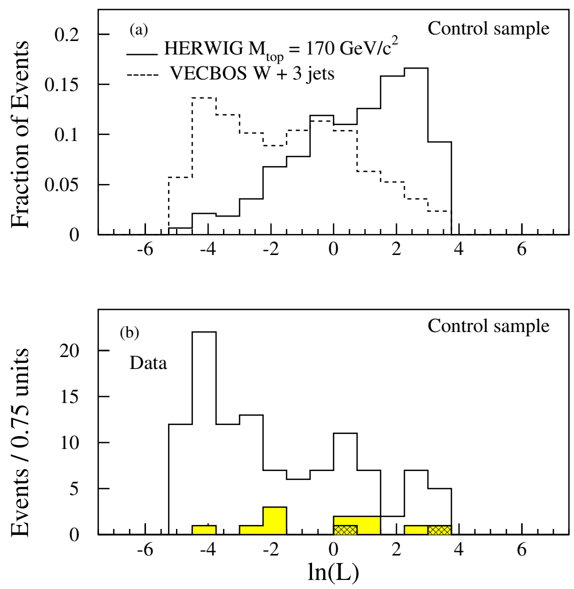

FIG. 91. The distribution in natural log-likelihood for events in the control sample. (a) Monte Carlo expectations for $W+$ jets (VECBOS) and $t\bar{t}$ (HERWIG); (b) Data. The lightly shaded histogram shows the b-tagged events. The darkly shaded histogram shows events with two b-tags. From the CDF collaboration, F. Abe *et al.*, 1995b. The integrated luminosity is 67 pb^{-1}.

calculation in the kinematic region most relevant for the top search.

D. Significance of the top signal

As discussed in Sections VIII.A, VIII.B, and VIII.C, the CDF and D0 top searches in a number of different channels find excesses of top-like events over the background predictions. The significance of the excess for a given channel is defined as the probability that a background fluctuation would yield a number of events equal to or larger than the number of observed events. This probability is calculated by convoluting the Poisson probability for the fluctuation of the mean expected number of background events with its uncertainty, which is assumed to be Gaussian.

When combining results from more than one channel, D0 and CDF use different procedures. In the D0 case, events from all channels as well as backgrounds from all channels are added, and the combined significance is defined as the probability that the sum of all the backgrounds fluctuates to give a total number of events greater than or equal the number of observed events. On the other hand, the CDF combined significance is defined as the probability that the product of the significances for the different channels be less than or equal to the measured value for this product. This is necessary since the CDF vertex-tag channel has so much better efficiency and signal to noise than the dilepton and (especially) the lepton-tag channels. In fact, if the D0 prescription were to be applied to compute the total significance of the CDF excesses in the three channels, the combined excess would appear less significant than the excess seen in the vertex-tag channel alone, despite the fact that excesses are seen in the other two channels as well. When combining different channels, correlations are accounted for. For example, both the CDF lepton and vertex tag searches are sensitive to the size of the W$Q\bar{Q}$ background, resulting in a correlation between significances in the two channels. These effects are taken into account using Monte Carlo simulations.

The significances for the CDF and D0 results are displayed in Table XVIII. These significances, which as discussed above are just probabilities, are also expressed in number of standard deviations (No. of σ). The number of σ corresponds to the point in a Gaussian probability function of mean zero and unit standard deviation where the integral of the probability function between that point and infinity is equal to the significance.

The results from both experiments are such that the probability that the data can be explained as background fluctuations is exceedingly small. We note that, in the calculation of the combined significance of their top observation, the CDF collaboration very conservatively does not include the excess of top-like events seen in their purely kinematic analyses of lepton + jets data (see Section VIII.C.2). Furthermore, as will be discussed in Section IX, both CDF and D0 find additional evidence for a $t\bar{t}$ contribution to their lepton + jet data samples in the top mass reconstruction analyses. To summarize, the data from the counting experiments at the Tevatron provide overwhelmingly convincing evidence for the existence of new physics. We shall show in the following section that the invariant mass and kinematics of this new physics are consistent with a top quark of $M_{top} \approx 175$ GeV/c^2.

Experiment	Channel	Events observed	Expected background	Significance	No. of σ
D0	Muon b-tag	6	1.2±0.2	2 x 10^{-3}	2.9σ
D0	Lepton + jets	8	1.9±0.5	2 x 10^{-3}	2.9σ
D0	Dileptons	3	0.7±0.2	3 x 10^{-2}	1.9σ
D0	All combined	17	3.8±0.6	2 x 10^{-6}	4.6σ
CDF	Vertex b-tag	21 (27)	6.7±2.1	2 x 10^{-5}	4.2σ
CDF	Lepton b-tag	22 (23)	15.4±2.0	6 x 10^{-2}	1.5σ
CDF	Dileptons	6	1.3±0.3	3 x 10^{-3}	2.7σ
CDF	All combined	43 (56)	23.4±2.9	1 x 10^{-6}	4.8σ

TABLE XVIII. CDF (F. Abe *et al.*, 1995a) and D0 (Abachi *et al.*, 1995b) event yields, background expectations, and significances of the observed excesses of top-like events in different channels. In the CDF b-tagging channels, we show both the number of events and, in brackets, the number of tags. There are 6 events which are tagged with both a vertex b-tag and a lepton b-tag in CDF. The two *all combined* entries for CDF data refer to 43 events and 56 *objects*, where an object is defined as either a dilepton event or a tag in a lepton + jets event. The CDF b-tag backgrounds are expressed in number of tags; the CDF all combined background is expressed in number of objects. Tags in CDF dilepton events are not included anywhere in this table.

E. Measurement of the $p\bar{p} \to t\bar{t}$ cross-section

The $t\bar{t}$ production cross-section is calculated from the luminosity, the background-subtracted event yields, the acceptances, and the $t\bar{t}$ decay branching fractions for the various channels. The calculated cross-section depends on the top mass, since the acceptances are in general also a function of the top mass.

The measurement is complicated by the fact that in some cases the expected number of background events depends on the cross-section itself. For example, in the CDF b-tag analysis the background due to $WQ\overline{Q}$, which is quoted in computing the significance of the $t\bar{t}$ observation, is calculated under the assumption that the pre-tag $W+ \geq 3$ jets sample does not contain any top events. Having established the existence of the top quark, this background estimate needs to be revised, since the untagged sample does indeed include a $t\bar{t}$ component. This is accomplished by first calculating the cross-section using the overestimated background contribution, then recalculating the background based on the value of the cross-section, and iterating until the result becomes stable.

The CDF and D0 $t\bar{t}$ production cross-sections, are listed in Table XIX, and displayed in Fig. 92. As discussed at the beginning of this Section, the cross-section calculation depends on the assumed value of M_{top}. Here we report $\sigma(p\bar{p} \to t\bar{t})$ computed at the values of M_{top} measured by the two collaborations, see Section IX. The CDF and D0 cross-sections reported here are obtained from data sets of 110 pb^{-1} and 100 pb^{-1} respectively.

The top mass dependence of the cross-section measurement is $\delta\sigma/\delta M_{top} \approx -0.05$ pb/GeV/c^2 (D0) and -0.04 pb/GeV/c^2 (CDF). For both experiments the dominant uncertainty on $\sigma(p\bar{p} \to t\bar{t})$ is due to the limited statistics of the data samples. Also, for both experiments the separate cross-section measurements in the different channels are nicely consistent with each other. The CDF measurement is lower than, although still consistent

Experiment	Top mass	Channel	Measured cross-section
D0	180 GeV/c^2	Muon tag	6.8 ± 3.2 pb
D0	180 GeV/c^2	Lepton + jets	3.9 ± 1.9 pb
D0	180 GeV/c^2	Dileptons	4.6 ± 3.1 pb
D0	180 GeV/c^2	All combined	4.7 ± 1.6 pb
D0	170 GeV/c^2	All combined	5.2 ± 1.8 pb
CDF	176 GeV/c^2	Vertex tag	$6.8^{+2.3}_{-1.8}$ pb
CDF	176 GeV/c^2	Lepton tag	$8.0^{+4.4}_{-3.6}$ pb
CDF	176 GeV/c^2	Dileptons	$9.3^{+4.4}_{-3.4}$ pb
CDF	176 GeV/c^2	All combined	$7.5^{+1.9}_{-1.6}$ pb

TABLE XIX. CDF (Tartarelli, 1996) and D0 (Narain, 1996; Klima, 1996) measurements of $\sigma(p\bar{p} \to t\bar{t})$ at a center-of-mass energy of 1.8 TeV. The integrated luminosities for these measurements are 110 pb^{-1} for CDF and 100 pb^{-1} for D0. Note that the most recent D0 top mass value is $M_{top} = 170 \pm 18$ GeV/c^2, see Section IX.A.4. Cross section values for this value of M_{top} for the individual channels have not been released by the D0 collaboration. Here we list these cross-sections at $M_{top} = 180$ GeV/c^2 to demonstrate the consistency between the measurements in the different channels.

with, the cross-section value of $13.9^{+6.1}_{-4.8}$ pb obtained from the analysis of the first 19 pb^{-1} of CDF data (F. Abe *et al.*, 1994a).

Both the CDF and D0 $t\bar{t}$ cross-section measurements are in agreement with the theoretical prediction. To summarize, both collaborations have not only reported excesses of top-like events in several different channels, but the sizes of these excesses are also consistent with each other. From these measurements, they have extracted values of $\sigma(p\bar{p} \to t\bar{t})$ which are consistent, within the quoted uncertainties, with Standard Model expectations.

IX. MEASUREMENT OF THE TOP QUARK MASS

The CDF and D0 top quark searches described in Section VIII yield an excess of top-like events over the background expectations. In this Section we will present measurements of the top mass performed on a sub-set of these events. As was discussed in Section III, the mass of the top quark is one of the free parameters of the Standard Model, and its value enters in the calculation of radiative corrections to a large number of electroweak observables. Comparison of the measurement of M_{top} with indirect determinations from electroweak measurements at LEP and SLC, as well as measurements of the W mass at the Tevatron and LEP200, and analysis of neutral current neutrino data, allow for rather stringent tests of the Standard Model.

There are a number of possible ways to extract the top mass from the CDF and D0 data. An indirect method is to simply compare the cross-section for the observed $t\bar{t}$ signal with its theoretical expectation, since the latter depends very strongly on the top mass, (see Fig. 92). However, it is more informative to *measure* both the top mass and the $t\bar{t}$ cross-section, and

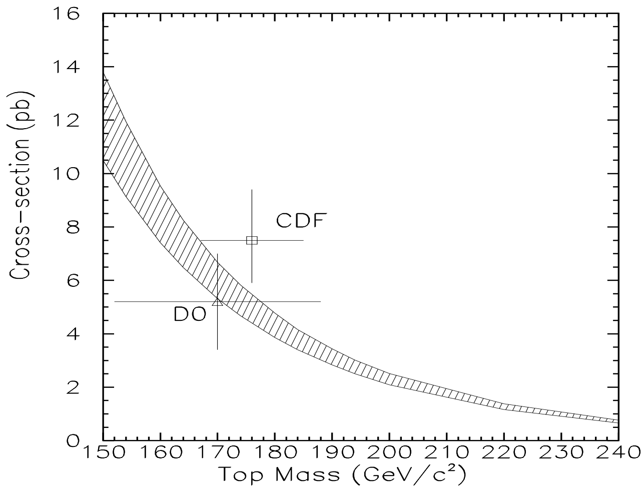

FIG. 92. Combined CDF and D0 top cross-section and mass measurements. (The mass measurements will be summarized in Section IX). Also shown, as a band, is the theoretical expectation for $\sigma(p\bar{p} \to t\bar{t})$ as a function of M_{top} with its uncertainty (Laenen, Smith, and van Neerven, 1994).

then compare with the theoretical prediction for $\sigma(t\bar{t})$. This approach results in a test of the QCD calculation of top production, and is sensitive to possible non-Standard Model production mechanisms for top quarks, see the discussion in Section X.

Both CDF (F. Abe *et al.*, 1994a and 1995a) and D0 (Abachi *et al.*, 1995b) have reported direct measurements of the top mass from lepton + jets data and these will be reviewed in Section IX.A. Other less direct methods to extract the value of M_{top} from both the lepton + jets data and the dilepton data will be summarized in Section IX.B. Finally, in Section IX.C, we will present results of attempts to reconstruct the W mass from $W \to q\bar{q}$ in lepton + jets events.

A. Direct measurements of the top quark mass from lepton + jets events

The method used by both CDF and D0 to measure the top quark mass is the standard method used in particle physics to measure particle masses, namely one measures the momenta of all the decay products, assigns masses to them, and then reconstructs the invariant mass of the original particle. In the case of top quarks, the decay products include neutrinos and hadron jets. The first example of the reconstruction of resonances using jets was UA2's observation of a bump consistent with the W and Z in the jet-jet invariant mass distribution (Alitti *et al.*, 1991a). In this case there was an an enormous background from QCD production of jets not involving a vector boson. The field of jet-spectroscopy is still in its infancy, although much progress has been made in the past year.

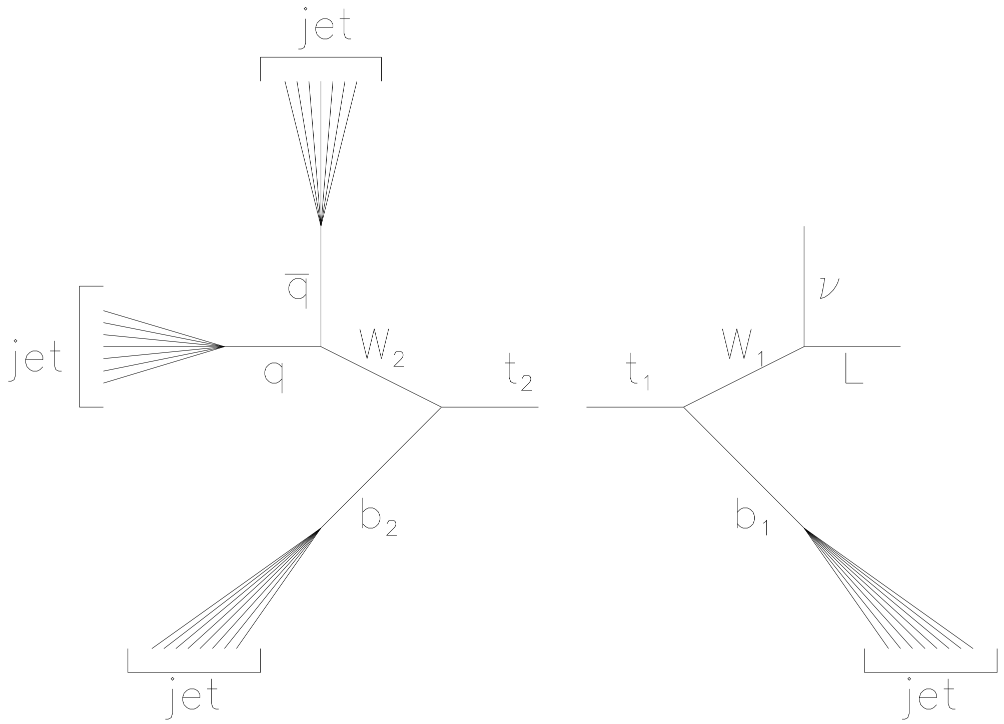

FIG. 93. Sketch of the $t\bar{t}$ decay chain in the lepton + jets channel.

1. Constrained fits, combinatorics, and top mass resolution

In the $t\bar{t} \to$ lepton + jets mode, one of the two top quarks (t_1) decays semi-leptonicaly and the other one (t_2) decays hadronicaly, (see Fig. 93) :

$$t_1 \to W_1 b_1 \quad ; \quad W_1 \to l\nu$$

$$t_2 \to W_2 b_2 \quad ; \quad W_2 \to q\bar{q}$$

The mass measurement is performed on the sample of events with a lepton, $\not{E}_{\mathrm{T}}$ and four jets. The four jets are identified with the four quarks in the final state (b_1, b_2, q and $\bar{q}$). Without further information there is no way of knowing which jet originates from which quark. All possible combinations must be considered. A constrained fit to the $t\bar{t}$ hypothesis is then performed for each jet-quark assignment in a given event, assuming energy-momentum conservation at each vertex in the $t\bar{t}$ decay chain. The fit uses the following constraints :

- The invariant mass of the jets assigned to the q and $\bar{q}$ is constrained to the W mass.
- The $\not{E}_{\mathrm{T}}$ gives the transverse momentum of the neutrino. The longitudinal momentum of the neutrino, $\mathrm{P}_{L\nu}$, is obtained by requiring the mass of the lepton and the neutrino to equal the W mass. This condition results in a quadratic equation for $\mathrm{P}_{L\nu}$, which has in general two distinct solutions.

- The invariant masses of the decay products of t_1 and t_2 must be equal, i.e. the invariant mass of the three jets assigned to b_2, q, and $\bar{q}$ (M_2) must be equal to the invariant mass (M_1) of the lepton, neutrino and fourth jet (b_1, see Fig. 93). The top mass for the jet-quark assignment under consideration is then $M_{top} = M_1 = M_2$.

All of the components of momentum for the final state particles are measured, except $P_{L\nu}$. With one unmeasured quantity and three constraints, the fit is a two-constraint (2C) fit. The constrained fit also yields a χ^2 for each combination which is a measure of the goodness-of-fit to the $t\bar{t}$ hypothesis. The fitted value of the top quark mass for a given combination is given by $M_{top} = M_1 = M_2$ at the point where χ^2 is minimized.

There are $4! = 24$ possible ways of assigning the four jets to the four final-state quarks. Since there are two solutions for $P_{L\nu}$, this would result in 24 x 2 = 48 configurations. However, the interchange of jet assignments between the q and $\bar{q}$ from the W has no effect (see Fig. 93), so that the number of truly distinct configurations is $48/2 = 24$. If one or more of the jets is b-tagged, the number of configurations can be reduced by allowing only configurations where b-tagged jets are associated with the b-quarks in the event. With one b-tagged jet, the number of combinations is twelve; with two b-tagged jets, this number is reduced to four.

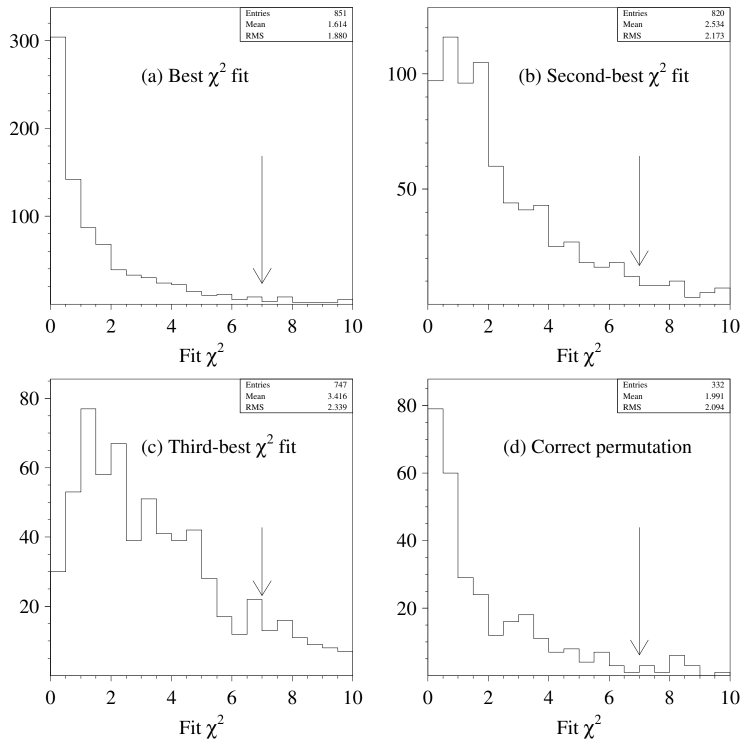

FIG. 94. Fit χ^2 distributions for (a) best, (b) second-best, (c) third-best, and (d) the correct jet permutation. For e+jets events, from the ISAJET Monte Carlo, M_{top}=180 GeV/c^2. The arrow shows the cut value. Note that the plot of correct permutations has less than half as many entries because only the cases in which a correct permutation could be found unambiguously from the Monte Carlo are included. From the D0 collaboration, Snyder, 1995a.

The large number of possible jet-quark assignments, the poor jet energy resolution (see Section V.B.2 and Fig. 32), and the effects of initial and final state gluon radiation, greatly complicate the top quark mass measurement. Monte Carlo studies indicate that there is often at least one combination with incorrect quark-jet assignments which yields a better fit to the $t\bar{t}$ hypothesis than the combination with the correct assignment, (see Fig. 94). Gluon radiation presents a problem because it can give rise to additional jets in the event. Both CDF and D0 consider only the four highest E_T jets in the event, since inclusion of a fifth jet would increase the number of possible combinations by a factor of five. However, if one of these four jets is from gluon radiation, the constrained fit will be operating on the wrong objects. Because of the poor energy resolution, the goodness-of-fit variable is not very effective at eliminating this kind of event from the data sample. An additional effect of gluon radiation is that the lepton + 4 jets sample also includes $t\bar{t}$ events from the *wrong* decay mode, for instance events of the type $t\bar{t} \to l\nu b\ \tau\nu\bar{b}$ can pass a lepton + 4 jets selection if both b-jets are found, the tau decays hadronically and is reconstructed as a jet, and an additional gluon jet is present.

The size of these effects depends somewhat on the details of the event selection. In the CDF analysis, Monte Carlo studies indicate that approximately 7% of $t\bar{t}$ lepton + 4 jets events are from the wrong decay mode, and of order 50% of the events have at least one of the four highest P_T jets from gluon radiation. In the remaining events, the combination with the lowest χ^2 corresponds to the correct parton-jet assignments only about one half of the times.

Constrained fits to incorrect parton-jet assignments or to $t\bar{t}$ events from the wrong decay mode, in general yield incorrect values of M_{top}. The CDF and D0 groups have chosen to deal with the problem of combinatorics in slightly different ways. In the CDF analysis, only the lowest χ^2 combination in a given event is considered. In the D0 analysis, the top quark mass for a given event is taken as the χ^2-weighted average of all combinations (up to three) that have acceptable values of χ^2. The advantage of the D0 approach is that the M_{top} value for a given event is more stable under small changes in the measurements or the fitting procedure. These changes can cause the fit to converge to a different jet-parton configuration, and result in a value of M_{top} which can be considerably different from the original.

Wrong combinations result in a significant broadening of the expected mass resolution, see Fig. 95. In CDF, the mass resolution for the correct jet assignment is expected to be 12 GeV/c^2. As a result of gluon radiation and wrong parton-jet assignments, the mass resolution is a factor of two worse, with significant non-Gaussian tails. Very similar results have also been reported by the D0 collaboration.

Despite the effects of gluon radiation and the high probability to choose a wrong combination, the peak in the mass distribution of Monte Carlo events is not shifted significantly, (see Fig. 95). This is partly because of order one-half of the wrong combinations involve interchange of one of the quarks from W decay (q or $\bar{q}$) with the b from the hadronic top decay (b_1, see Fig. 93). For this class of events, the reconstructed top mass distribution is broader but still peaks at the correct value.

It may be possible to reduce the effect of wrong combinations by including more information in the event fitting procedure. Examples of additional pieces of information that could be included are the expected angular distributions derived from the V-A structure of the top quark decay or the rapidity distributions of top quarks predicted by the $t\bar{t}$ cross-section

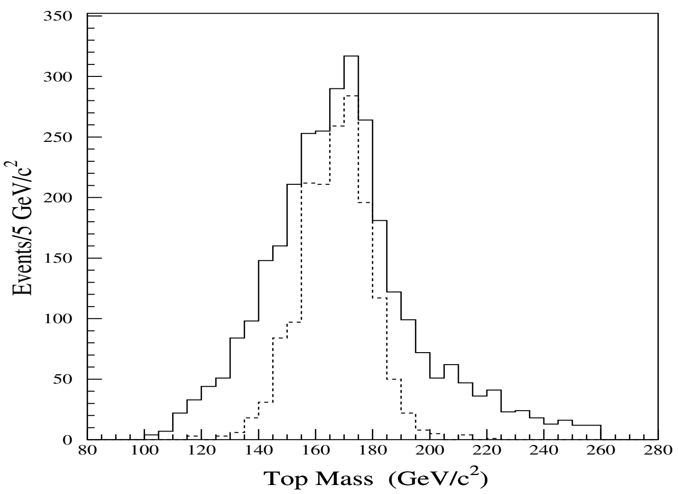

FIG. 95. Reconstructed top mass distribution for Monte Carlo events generated with the HERWIG Monte Carlo program, and simulated with the CDF detector simulation. The input value of the top mass in the Monte Carlo is $M_{top} = 170$ GeV/c^2. The solid line corresponds to the result of the constrained fit when requiring that one of the b-jets is a b in the fit. The dashed histogram refers to the fit with the correct assignment for each of the jets. The width of the top quark, which for this top mass is $\Gamma(t) \approx 1$ GeV/c^2 see Fig. 24, is negligible compared to the experimental resolution. From the CDF collaboration, F. Abe *et al.*, 1994a.

calculation (Kondo, 1991; Goldstein, Sliwa, and Dalitz, 1993).

Another effect of the large number of combinations and the poor jet energy resolution is that the χ^2 goodness-of-fit variable does not provide significant background rejection. (If it did, this variable would have been used to separate the top signal from the background). As discussed in Sections V.E.1, VIII.B, and VIII.C, the main background to the lepton + jets top signal is due to $W+$ jets production. In a $W+$ 4 jets event, it is almost always possible to find one jet-quark assignment with χ^2 low enough to be consistent with the $t\bar{t}$ hypothesis. Therefore, in order to perform the top mass measurement, both the background contamination of the event sample, and the mass distribution of the background events, need to be understood.

2. CDF and D0 top mass measurements

The CDF and D0 top mass measurements are based on the constrained fit procedure described in the previous Section. What is measured in these detectors is the energy and direction of the jets. In order to measure the top mass, the jet energies must be corrected to infer the original momentum of the partons. The correction procedure takes into account effects of non-linearities in the hadron energy response of the calorimeters, underlying event contributions to the energy of the calorimeter cluster, and gluon radiation outside the clustering cone. Special corrections are applied to lepton-tagged b-jets, since additional energy is carried away by the neutrino emitted in the semileptonic b-decay (typically a few GeV).

A value of M_{top} is calculated for each event using the constrained-fit procedure described above. Events are rejected if the fit χ^2 is inconsistent with the $t\bar{t} \rightarrow$ lepton + jets hypothesis. The top quark mass is extracted by performing a likelihood fit to the M_{top} distribution for the remaining events. This M_{top} distribution is fit to the sum of background and $t\bar{t}$ components, with the value of the top quark mass allowed to vary. The M_{top} distribution for the dominant background, ($W+$ 4 jets events), is obtained by performing the same constrained fit procedure on a sample of events obtained from the VECBOS Monte Carlo and the detector simulation. The shape of the expected M_{top} distribution, as a function of the mass of the top quark, is also taken from Monte Carlo event generators (ISAJET, HERWIG, or PYTHIA) and the detector simulation. In the fit, the size of the background contribution can be constrained, within errors, to its calculated value, or can be left free to float. In the latter case, the size of the background contribution returned by the fit serves as a consistency check of the procedure.

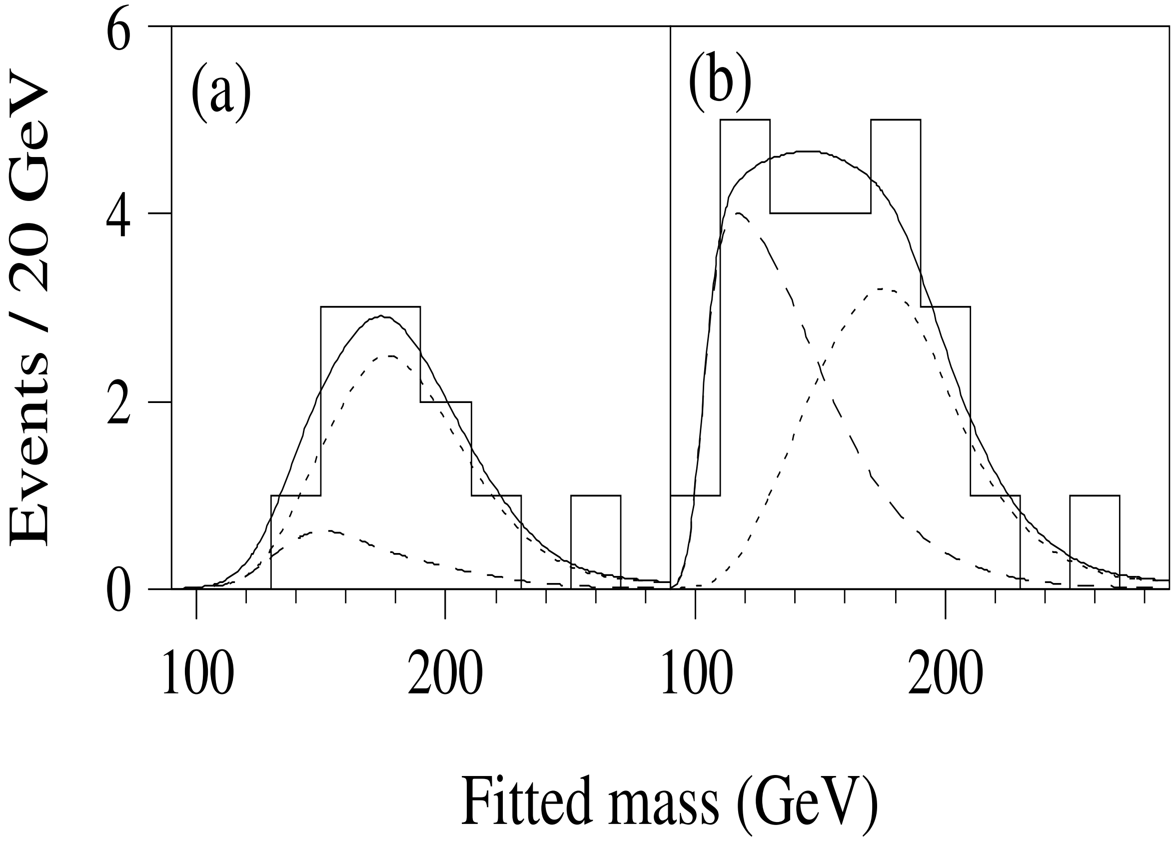

FIG. 96. Mass distribution for D0 top candidate events (histogram) compared with the expected mass distribution for 199 GeV/c^2 top quark events (dotted curve), background (dashed curve), and the sum of top + background (solid curve) for (a) standard and (b) loose event selection. b-tagging information is used when available. From Abachi *et al.*, 1995b. The integrated luminosity is ≈ 45 pb^{-1}.

The results of the likelihood fit from the D0 collaboration are shown in Fig. 96(a) and 96(b) for two different event selections, *tight* and *loose*. In both cases the four jets are required to have $E_T > 15$ GeV. The tight selection includes requirements on H_T and aplanarity. The tight sample includes the eight lepton + four jets events from the analysis described in Section VIII.C, as well as the 6 b-tagged events from Section VIII.B. Only 11 out of these 14 events yield an acceptable fit to the $t\bar{t}$ hypothesis. For the loose selection, the H_T requirement is removed and the aplanarity requirement is loosened. The H_T requirement selects events with high E_T jets, and introduces a bias that favors events with high reconstructed top mass. By removing this requirement, however, the background contribution is enhanced. The number of events increases from 14 to 27; 24 of these have at least one combination with good χ^2 (Snyder, 1995a). As discussed in Section V.B and illustrated in Fig. 33, in $t\bar{t} \to$ lepton + jets events there is a significant probability for two quarks in the final state to merge into a single jet. To minimize this effect, the jet-cone clustering radius (ΔR, see Section V.B) in the D0 mass reconstruction is changed from the 0.5 used in the selection of the top signal to 0.3. Likelihood fits to the two distributions result in top mass values of $M_{top} = 199^{+31}_{-25}$ GeV/c^2 and $M_{top} = 199^{+19}_{-21}$ GeV/c^2 for the tight and loose selections respectively (statistical errors only). The M_{top} data distributions are not well described by the background hypothesis alone. This provides further kinematic evidence for the existence of the top quark.

The CDF top observation in the lepton + jets channel was based on a sample of b-tagged events with at least three jets of uncorrected $E_T > 15$ GeV, clustered with a cone of radius $\Delta R = 0.4$. As it is clear from Fig. 93, the constrained fit can only be applied to events with at least four jets. Therefore, the CDF mass measurement is performed on the sub-sample of events with a fourth jet. To maintain high efficiency, the E_T threshold on the fourth jet is lowered from 15 to 8 GeV (uncorrected). We stress that uncorrected jet energies are used at the event-selection stage only; for fitting purposes, all jet energies are corrected, see the discussion in Section IX.A.3. In Fig. 97 we show the M_{top} distribution of the pre-tag CDF lepton + 4 jets sample. Based on the CDF $t\bar{t}$ cross-section measurement, this sample is expected to be a mixture of approximately 30% $t\bar{t}$ and 70% $W+$ jets. The probability for the shape of the data M_{top} distribution to be consistent with background only is approximately 2%. Hence, just as in the D0 case, this distribution provides additional evidence for the top quark. By demanding a b-tag, the bulk of events at low M_{top} is removed, leaving a cluster of events between $M_{top} = 150$ and 210 GeV/c^2, see Fig. 98. The result of the likelihood fit to these events is $M_{top} = 176 \pm 8$ GeV/c^2 (statistical error only).

When including systematic effects, the mass values reported by the two collaborations are $M_{top} = 199^{+19}_{-21}$(stat.)$\pm$22(syst.) GeV/c^2 (D0) and $M_{top} = 176 \pm 8$(stat.)$\pm$10(syst.) GeV/c^2 (CDF). The results are consistent with each other. In the following Section we will discuss the important issue of systematic uncertainties.

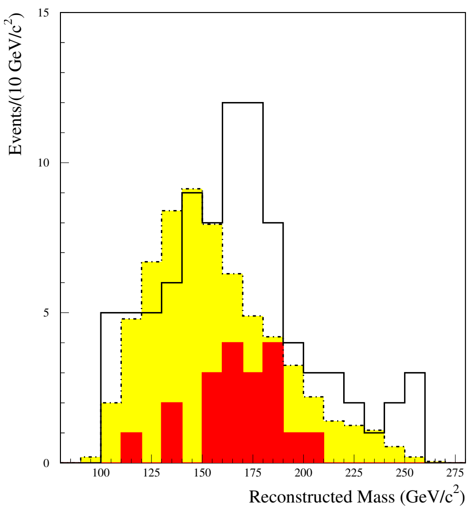

FIG. 97. Mass distribution for the 88 CDF lepton + $\geq$ 4 jets events with a good χ^2 fit to the $t\bar{t}$ hypothesis, before the b-tag requirement (solid line). The darkly shaded histogram is for the 19 events with a b-tag. The expected $W+$ 4 jets contribution to the pre-tag sample is shown in the lightly shaded histogram. From F. Abe *et al.*, 1995a. The integrated luminosity is 67 pb^{-1}.

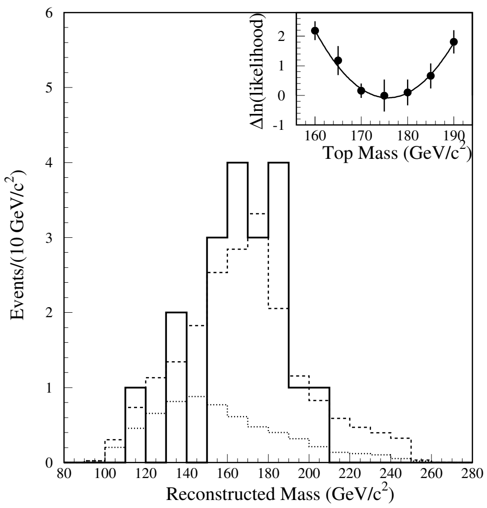

FIG. 98. Mass distribution for the 19 CDF b-tagged lepton + $\geq$ 4 jets events with a good χ^2 fit to the $t\bar{t}$ hypothesis (solid). Also shown are the background shape (dotted), and the sum of background and $t\bar{t}$ Monte Carlo (dashed) for M$_{top}$ = 175 GeV/c^2. The inset shows the likelihood fit used to determine the top mass. From F. Abe *et al.*, 1995a. The integrated luminosity is 67 pb^{-1}.

Although the data samples of top candidates are rather small, the size of the statistical error on the top quark mass measurement is already comparable to the size of the systematic uncertainties. It is expected that in the next decade much larger $t\bar{t}$ samples will be available, see Section X. The systematic uncertainties will then be the limiting factor in the precision of the top mass measurement.

The dominant uncertainty in the top mass measurement is due to the uncertainty in the jet energy scale, i.e. to the transfer function (*correction factor*) that relates the measured jet energies to the energies of the original quarks from top decay. This uncertainty has two components, (i) an instrumental uncertainty related to the response of the calorimeter to hadrons, and (ii) an uncertainty in the understanding of the fragmentation and gluon radiation processes. In order to discuss these systematic uncertainties, we begin by describing the many steps in the jet energy correction procedure (F. Abe *et al.*, 1992d and 1993c; Abachi *et al.*, 1995d).

The jet energy response is in general not uniform across the detector because, for example, of cracks at the boundaries between calorimeter modules. The first task of the correction procedure is to equalize response across the calorimeter. The size of the effect is measured *in-situ* by di-jet or photon balancing techniques. Di-jet balancing is performed on a sample of $p\bar{p} \rightarrow 2$ jets events, with one jet restricted to a well-understood region of the calorimeter. Since the transverse energies of the two jets are expected to be equal, any inbalance as a function of the position of the second jet is a measure of the position-dependent non-uniformity of the calorimeter response. A similar study can be performed using $p\bar{p} \rightarrow \gamma +$ jet events. In these events the accurate measurement of the E_T of the photon can be compared to the measurement of the jet E_T. These effects can be measured, and hence corrected for, with high precision, because of the very large number of di-jet and photon-jet events that can be used for this study.

The jet cluster will in general include energy deposited from particles unrelated to the parent parton, for example particles from the underlying event. The jet energy is therefore corrected by subtracting off the average underlying event deposition as measured in minimum bias events. For jets clustered with a cone radius $\Delta R = 0.4$, this correction amounts to approximately 600 MeV for the CDF detector. Note that in $t\bar{t}$ events the amount of extra energy can be higher, because of cross-talk between the many jets in the final state. An additional, Monte Carlo based, correction for this effect has been developed by the CDF collaboration. A further correction needs to be applied in D0 due to noise from radioactivity of the uranium plates used in the calorimeter.

The next ingredient in the jet energy correction procedure involves understanding the absolute energy response of the calorimeter. The response to individual hadrons is measured in test-beams. In CDF the hadron response of the calorimeter as a function of momentum is also obtained from samples of isolated particles from $p\bar{p}$ collisions. The detector simulation is adjusted to incorporate information from these measurements. Finally, the jet energy scale is measured by simulating the calorimeter response to jets generated using a QCD-based model of jet fragmentation.

The absolute energy scale can also be derived from photon balancing, since the energy of the photon is precisely measured in the electromagnetic calorimeter. The electromagnetic

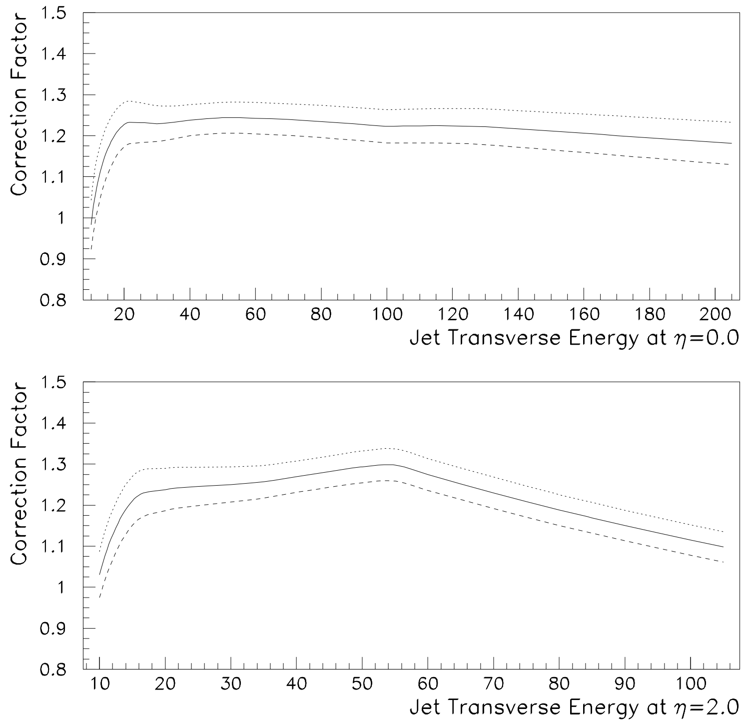

FIG. 99. D0 energy scale correction for jets as a function of jet transverse energy in the central and forward regions. Results are for jets reconstructed using a cone-size ΔR= 0.5. The dashed curves represent the error bands. From Abachi *et al.*, 1995d.

calorimeter is precisely calibrated by studying the distribution of E/P for electrons (CDF), or from reconstruction of the $Z \to ee$ resonance (D0). As we will discuss shortly, the photon balancing technique simultaneously tests instrumental as well as gluon radiation effects.

Finally, in order to go back to the original parton energy, an additional correction has to be applied for energy radiated outside the clustering cone, or carried away by low momentum hadrons swept away by the magnetic field (CDF). This correction is based on a Monte Carlo model of the QCD process. The overall jet energy correction factors are displayed in Fig. 99 and Fig. 100 for D0 and CDF respectively. The observed jet energies are to be multiplied by these correction factors to obtain the corrected energy.

Photon-jet balancing provides a powerful probe of the behavior of the overall jet energy correction function, (see Fig. 101). Unfortunately this test is not free from its own systematic uncertainties. Photon samples collected at the collider are contaminated at about the 50% level by two-jet events, with one of the jets fragmenting to a high momentum π^0 or η, which is misidentified as a single photon. In these cases the transverse energy of the photon candidate is not expected to equal the transverse energy of the recoiling jet, because of the presence of additional fragmentation hadrons in the jet that fakes the photon signature. Furthermore the balancing results can be affected by undetected low-energy initial-state gluon radiation. It is estimated that these effects introduce an uncertainty of order 5% on the determination of the absolute energy scale. Similar studies are performed using $Z+$ jet

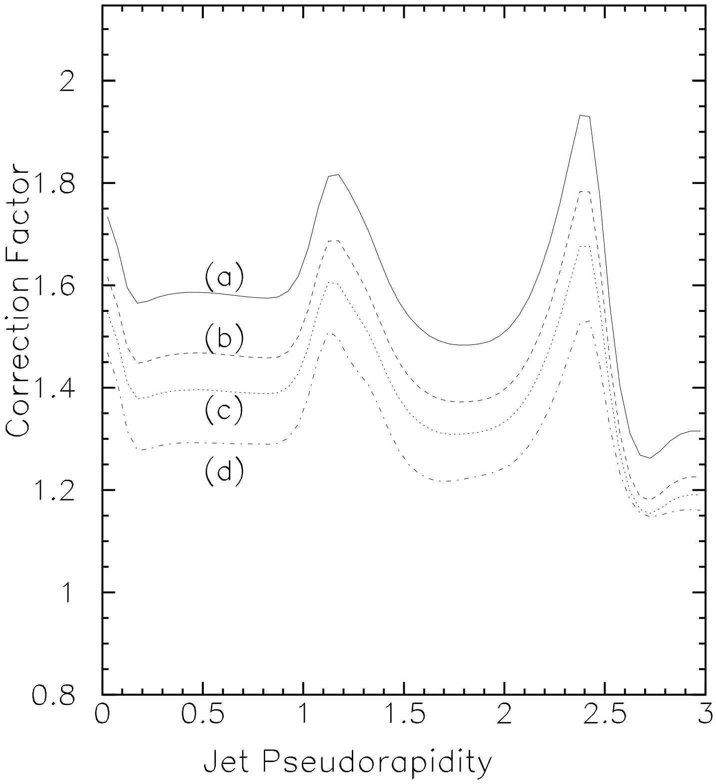

FIG. 100. CDF energy scale correction for jets as a function of jet pseudorapidity. Results are for jets reconstructed using a cone-size $\Delta R = 0.4$. (a) observed $E_T = 15$ GeV; (b) observed $E_T = 30$ GeV; (c) observed $E_T = 50$ GeV; (d) observed $E_T = 100$ GeV. The cracks between calorimeter modules (at $\eta \approx 0., 1.1, 2.4$) are apparent.

events, (see Fig. 102). The background effects which systematically limit the usefulness of photon-jet balancing are not present in this case; however, the available statistics are considerably lower.

The correction procedure described above applies to gluon and light-quark jets. Monte Carlo studies show no significant difference for b-jets, except in the case of semileptonic decays where an additional correction for the undetected neutrino needs to be applied.

The uncertainty in the jet energy scale for both the CDF and D0 mass analyses is estimated to be 10%. This value is somewhat larger than one would infer from photon-jet and Z-jet balancing studies, (see Fig. 101 and Fig. 102). There are however additional questions concerning the applicability of this correction procedure to the hadronic environment in top events which contribute to the 10% uncertainty estimate. The 10% jet energy scale uncertainty translates to a top mass uncertainty of 8 GeV/c^2 and 21 GeV/c^2 for CDF and D0 respectively. The difference between the two experiments in the size of the reported M_{top} uncertainties is not fully understood at this time.

There are additional smaller systematic uncertainties on the top mass measurement. A related uncertainty comes from the Monte Carlo modeling of gluon radiation in $t\bar{t}$ events. As was discussed in the previous Section, gluon radiation broadens the reconstructed M_{top} distribution. Since the top mass is extracted from a fit to the M_{top} data based on the

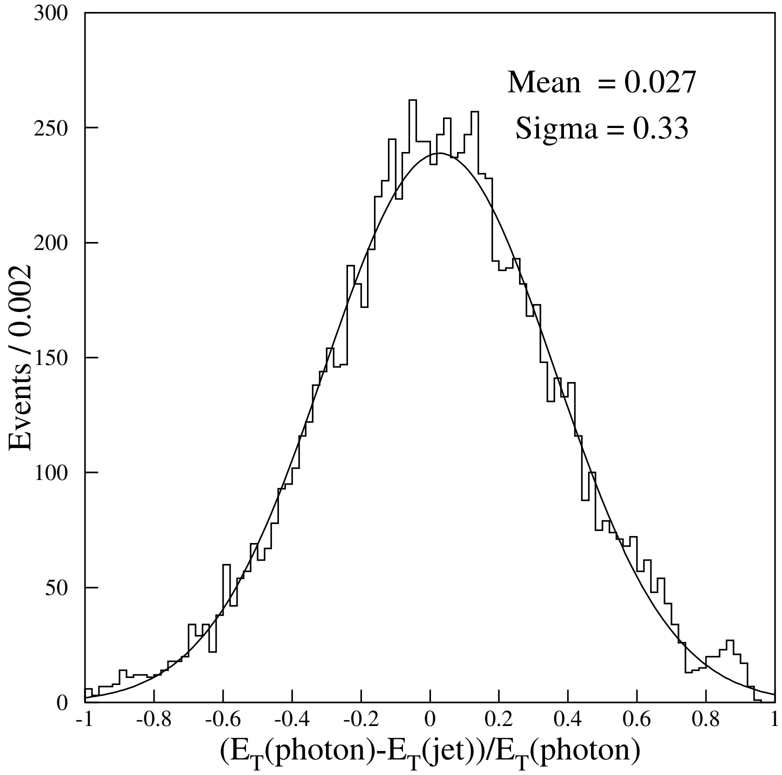

FIG. 101. Δ = (E$_T$ (photon) - E$_T$ (recoiling-jet))/E$_T$ (photon). The jet transverse energy is corrected. Jets are clustered in a cone ΔR = 0.4. From the CDF collaboration, F. Abe *et al.*, 1994a.

expected $t\bar{t}$ M$_{top}$ distribution, different assumptions on its shape can result in shifts of the measured top mass. For example, differences between the ISAJET and HERWIG models result in shifts of 4 and 1 GeV/c^2 for D0 and CDF respectively. Further uncertainties at the 1-2 GeV/c^2 level are present in the CDF measurement from uncertainties in the background shape, which is taken mostly from the VECBOS Monte Carlo, as well as the details of the likelihood fitting technique.

The CDF and D0 M$_{top}$ measurements are the first examples of the application of jet spectroscopy techniques to the determination of the mass of an elementary particle. The understanding and control of the systematic uncertainties due to the jet energy measurements are expected to improve in the future. This will be crucial to allow for more precise measurements of the top mass. We will discuss a number of possible approaches in Section X.

4. Updated CDF and D0 top mass measurements

As this review article was being completed, both the CDF (Tartarelli, 1996) and D0 (Narain, 1996) top mass results have been updated. In both experiments, the statistical

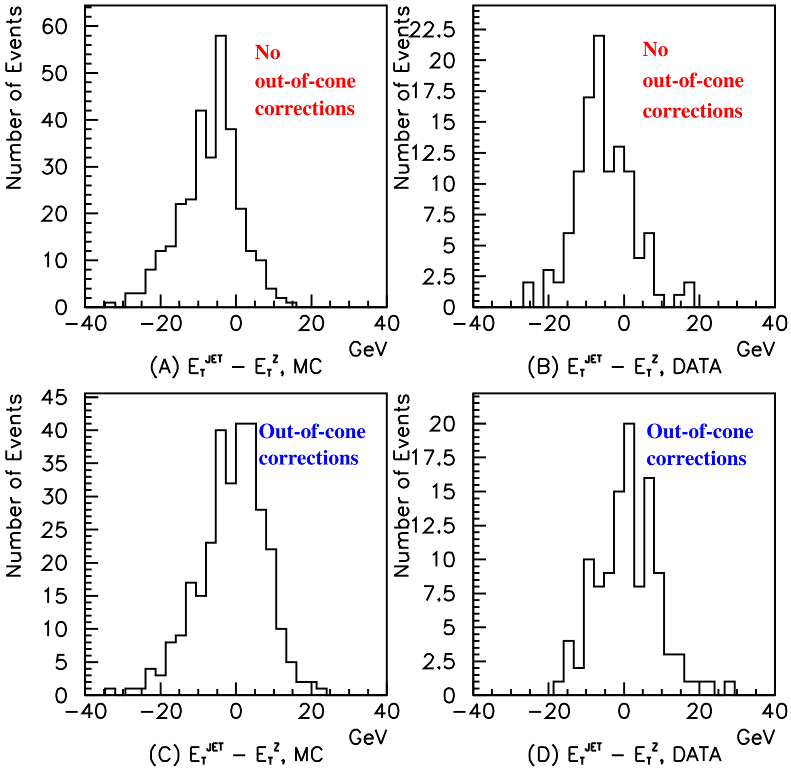

FIG. 102. Difference between the transverse energy of the electron pair and the jet in $(Z \to ee) + 1$ jet events. For Monte Carlo and data, with and without out-of-cone corrections, but including all other corrections. The minimum jet E_T is 10 GeV. Jets are clustered in a cone $\Delta R = 0.3$. From the D0 collaboration, Snyder, 1995a.

errors have decreased due to the larger data samples and, more importantly, the systematic uncertainties have been reduced as a result of more detailed studies of the jet energy scales in the two experiments. Since numerically the D0 result is somewhat different than the 1995 result discussed in Section IX.A.2, we briefly include these updated results here.

The new D0 measurement is based on an integrated luminosity of 100 pb^{-1}. Besides the improvement in statistics, there are four differences between the old and new D0 mass measurements: (i) the selection of the sample on which the mass fit is performed has been changed, (ii) an error in the out-of-cone jet energy corrections has been fixed, (iii) the HERWIG Monte Carlo is used instead of ISAJET, and (iv) the jet energy scale has been shifted downwards by 5%.

The new sample is derived from the loose lepton + four jets sample, removing the aplanarity cut. The sample is then split into two pieces, those events with and without a low P_T muon b-tag. The untagged events must satisfy two additional requirements: (i) the transverse energy of the leptonic W must be greater than 60 GeV, and (ii) the pseudorapidity of the W must be in the interval $\pm$ 2. The longitudinal momentum of the neutrino from the W is chosen from two possibilities as the one having the lowest momentum. Furthermore, the events are required to pass a kinematic liklihood test. This was done in order to reduce background for the loose sample, while reducing the mass bias due to the previous H_T

Source	M_{top} uncertainty
Jet energy scale (4% $\pm$ 1 GeV)	7 GeV/c^2
Different Monte Carlo $t\bar{t}$ generators	6 GeV/c^2
Fitting	3 GeV/c^2
Background uncertainty	2 GeV/c^2
Total	10 GeV/c^2

TABLE XX. Systematic uncertainties in the updated D0 mass measurement. From Narain, 1996.

Source	M_{top} uncertainty
Jet energy scale (detector effects)	3.1 GeV/c^2
Soft gluon effects	1.9 GeV/c^2
Hard gluon effects	3.6 GeV/c^2
Different Monte Carlo $t\bar{t}$ generators	0.9 GeV/c^2
b-tagging bias	2.3 GeV/c^2
Background spectrum	1.6 GeV/c^2
Fit configuration	2.5 GeV/c^2
Likelihood method	2.0 GeV/c^2
Monte Carlo statistics	2.3 GeV/c^2
Total	7.1 GeV/c^2

TABLE XXI. Systematic uncertainties in the updated CDF mass measurement. From Tartarelli, 1996.

requirement. No further requirements are made on the sample with a b-tag, except for additional improvements to the algorithm for removing $Z \to \mu\mu$, and for the application of a tighter low P_T muon selection.

This analysis results in 30 events which satisfy the fit χ^2, five of which have a b-tagged jet. The background in this sample is estimated to be 17.4 $\pm$ 2.2 events; the fit is shown in Fig. 103, and gives $M_{top} = 170 \pm 15$(stat.) ± 10(syst.) GeV/c^2. This is to be compared with the earlier result $M_{top} = 199^{+19}_{-21}$(stat.)$\pm$22(syst.) GeV/c^2. The systematic uncertainties are summarized in Table XX.

The updated CDF measurement, based on an integrated luminosity of 110 pb^{-1}, is performed in the same manner as described in Section IX.A.2. The result is $M_{top} = 176 \pm 6$(stat.)$\pm$7(syst.) GeV/c^2; the systematic uncertainties are summarized in Table XXI.

The combined top mass measurement from the two Tevatron collaborations is $M_{top} = 175 \pm 8$ GeV/c^2. Here we have added the errors in quadrature and neglected correlations in the systematic uncertainties. These correlations are due, for example, to the modelling of $t\bar{t}$ production, and to the common assumptions made by the two collaborations in the determination of the jet energy scale.

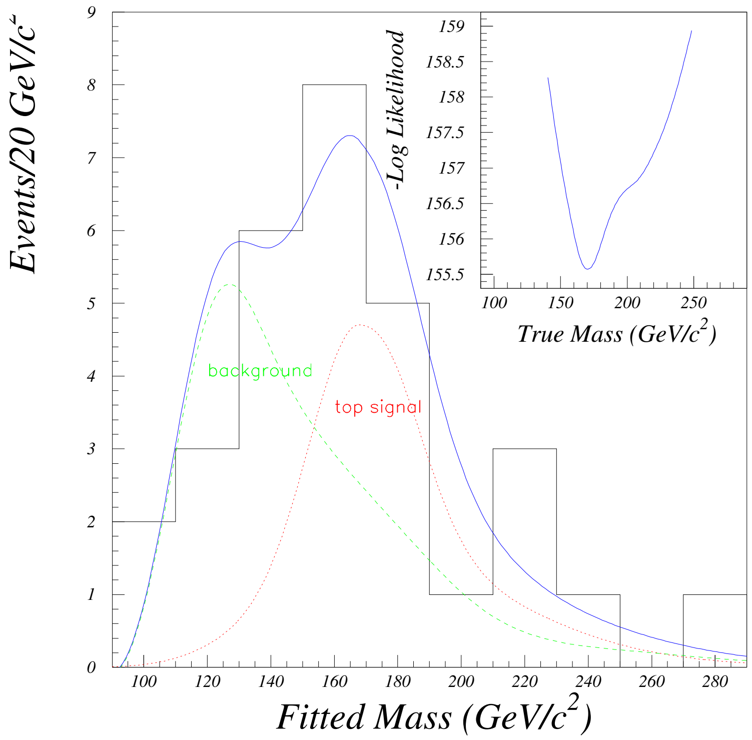

FIG. 103. Mass distribution for the 30 D0 lepton + ≥ 4 jets events with a good χ^2 fit to the $t\bar{t}$ hypothesis, from the 100 pb^{-1} data sample. The solid line is a fit to top plus expected background; the dashed line is the expected background from VECBOS (W + jets) and QCD multi-jet background; the dotted line is the fitted top contribution. The inset shows the liklihood distribution. From Narain, 1996.

B. Top mass from dilepton events and kinematic distributions

The top mass can also be reconstructed, in a less direct way, from dilepton events (Dalitz and Goldstein, 1992; Kondo, 1988 and 1991). In a $t\bar{t}$ dilepton event, both top quarks decay semi-leptonicaly :

$$t_1 \to W_1 b_1 \quad ; \quad W_1 \to l_1 \nu_1$$

$$t_2 \to W_2 b_2 \quad ; \quad W_2 \to l_2 \nu_2$$

Because of the presence of two neutrinos, a direct event-by-event reconstruction of the top mass based only on the measurements of the momenta of the leptons and the jets is not possible. The system is underconstrained, as can be seen from a simple accounting of the degrees of freedom. To fully describe the event, one needs the momenta of all the quarks and leptons in the final state. The momenta of the charged leptons are measured, and those of the quarks are inferred from the jet energies. Six parameters are needed to fully describe the two neutrinos; only two measurements (from the two components of $\not{E}_{\mathrm{T}}$), and three constraints are available : Mass$(l_1\nu_1)$ = M_W; Mass$(l_2\nu_2)$ = M_W; Mass$(l_1\nu_1 b_1)$ = Mass$(l_2\nu_2 b_2)$. This leaves $6-5 = 1$ parameter undetermined. In order to measure the top mass, additional information need to be included. Possibilities include the Standard Model V-A expectations for the angular distributions in the top decay chain, or theoretical expectations for the kinematic properties of the produced t and $\bar{t}$.

The D0 collaboration (Snyder, 1995b) recently reported a preliminary measurement of the top mass from dilepton events. The D0 dilepton mass measurement uses five dilepton events. It is based on a data sample with a higher integrated luminosity than the D0 dilepton top search described in Section VIII.A which yielded three candidate events.

The top quark mass reconstruction for a single event goes as follows. By **assuming** a value of M_{top}, and for a given jet-b-quark assignment, the momenta of ν_1 and ν_2 are determined up to a possible four-fold ambiguity from the two quadratic constraints $\mathrm{M}^2(l_1\nu_1) = \mathrm{M}_W^2$ and $\mathrm{M}^2(l_2\nu_2) = \mathrm{M}_W^2$. For each configuration (two jet-b-quark assignments, and possible four-fold neutrino ambiguity), the event is fully reconstructed. A probability (Prob_{lep}) is assigned to each configuration based on the energy of the leptons in the rest frame of the top quarks. This probability is calculated for the assumed top mass, and is based on the expected structure of the decay. The momentum fractions x_1 and x_2 of the incoming quarks q_1 and $\bar{q}_2$ in the reaction $q_1 + \bar{q}_2 \to t\bar{t}$ are also reconstructed from the invariant mass ($\mathrm{M}_{t\bar{t}}$) and momentum ($\mathrm{P}_{t\bar{t}}$) of the $t\bar{t}$ system. Modulo the effects of gluon radiation, x_1 and x_2 can be obtained from $\mathrm{M}_{t\bar{t}} = \sqrt{x_1 x_2 s}$ and $\mathrm{P}_{t\bar{t}} = 0.5\sqrt{s}(x_1 - x_2)$, where $\sqrt{s} = 1.8$ TeV is the center-of-mass energy of the $p\bar{p}$ collision. An additional probability (Prob_x) is assigned to the configuration, still as a function of the assumed top mass, based on the parametrization of the parton distribution functions at momentum fractions $x = x_1$ and $x = x_2$, (see Fig. 19). Because the parton distribution functions are decreasing functions of x, Prob_x includes a correction to remove biases towards low values of M_{top}. The total probability for the configuration is given by the product $\mathrm{Prob}_{lep}\mathrm{Prob}_x$. The total probability for the event is the sum of the probabilities for all possible configurations. By varying the value of the assumed top mass, this procedure yields a probability distribution for each event as a function of top mass. To include resolution effects, the procedure is repeated many times after smearing the measurements of the lepton and jet momenta according to their expected resolutions. The total probability distribution for a single event is then defined as the sum of the probability distributions for the smeared events. An event top mass value is defined as the value of M_{top} at which the probability distribution is maximum (M_{peak}). Finally, the top mass is extracted from likelihood fits of the data M_{peak} distribution to the superposition of the expected $t\bar{t}$ and background contributions, (see Fig 104).

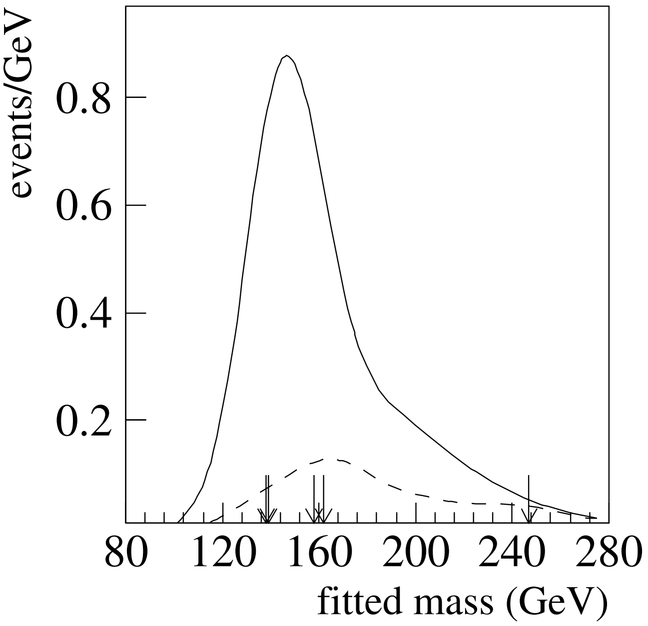

FIG. 104. Dilepton mass measurement from the D0 experiment. The arrows show the M_{peak} values for the five D0 dilepton candidate events. The solid curve is the expected signal distribution for $M_{top} = 145$ GeV/c^2, the dashed curve is the expected background distribution. See text for details. From Snyder, 1995b.

The preliminary D0 result for this procedure is $M_{top} = 145 \pm 25(\text{stat.}) \pm 20(\text{syst.})$ GeV/c^2. The systematic uncertainties include energy scale effects, Monte Carlo modeling, and uncertainties in the background contributions to the fit. Within the large errors, this value is consistent with both the CDF ($M_{top} = 176 \pm 9$ GeV/c^2) and D0 ($M_{top} = 170 \pm 18$ GeV/c^2) measurements in the lepton + jets channel described in Section IX.A.4.

A number of kinematic quantities in both dilepton and lepton + jet events have also been shown to be sensitive to the top mass (see for example Baer *et al.*, 1990). It is then in principle possible to perform a measurement of the top mass by comparing kinematic distributions to expectations for $t\bar{t}$. Some possibilities are the event transverse mass in dilepton events, the mean of the lepton-b mass, the transverse momentum of b-jets, or the total transverse energy, (see Fig. 105).

These more indirect measurements are less statistically powerful than the direct measurement of the top mass described in Section IX.A, since the mass peak used in the direct measurement provides optimal discrimination between different M_{top} hypotheses. However, indirect measurements are sensitive to different systematic effects. For instance, the combi-

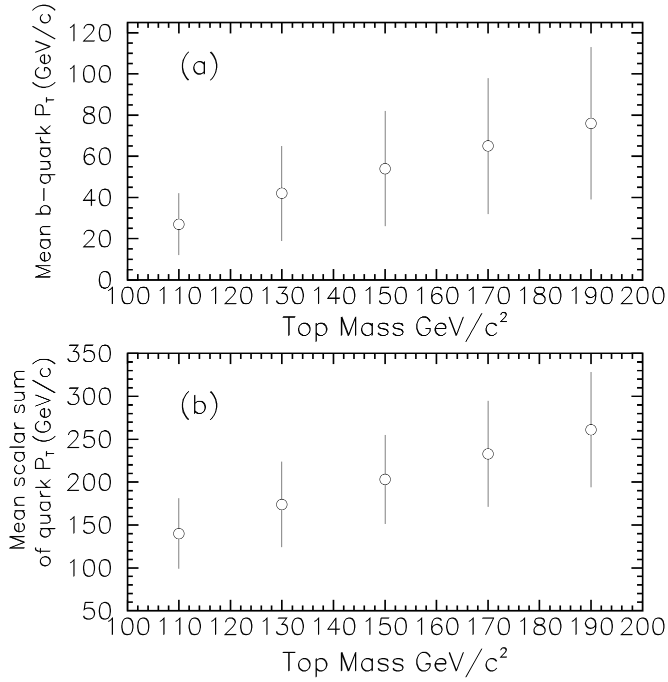

FIG. 105. Predictions from the ISAJET $p\bar{p} \to t\bar{t}$ Monte Carlo at $\sqrt{s} = 1.8$ TeV, as a function of the top mass, for (a) the mean transverse momentum of b-quarks, and (b) the mean of the scalar sum of the transverse momenta of the four quarks in lepton + jets events. The vertical error bars represent the expected RMS for these quantities.

natorics problem which plagues the direct top mass measurement, would not play a role in most of these techniques. A measurement of the top mass based on the b-quark transverse momentum spectrum or the b-lepton invariant mass, is almost entirely independent of initial state radiation in $t\bar{t}$ events.

The CDF collaboration has also reported measurements of the top mass based on kinematic distributions in both dilepton events (Tartarelli, 1996) and lepton + jets events (F. Abe *et al.*, 1995c). The dilepton mass determination is based on a fit to the jet E_T spectrum in these events and yields $M_{top} = 159^{+24}_{-22}(\text{stat.}) \pm 17(\text{syst.})$ GeV/c^2. The lepton + jet measurement is based on a fit to the the total transverse energy distribution (see Section VIII.C), and gives $M_{top} = 180 \pm 12(\text{stat.})^{+19}_{-15}(\text{syst.})$ GeV/c^2. Both these results are in agreement with the results derived by direct mass reconstruction techniques.

The direct top mass measurement in b-tagged lepton + jets events is, and is likely to remain, the method of choice for determining the top mass. Nevertheless, alternative methods such as the under-constrained dilepton mass reconstruction or methods based on kinematic distributions, serve as useful consistency checks.

C. Reconstruction of the W mass from hadronic decays in lepton + jets events

In a $t\bar{t} \rightarrow$ lepton + jet event, one of the two W bosons from the top decay chain is expected to decay hadronically ($W \rightarrow q\bar{q}$, see Fig. 93). Both the CDF and D0 collaborations have reported evidence for this decay mode by reconstructing a peak in the invariant mass distribution of two jets in the event. Hadronic W reconstruction is interesting for two reasons. First of all, the presence of such a peak in the data is further strong evidence that the excess of events over the background prediction is indeed due to $t\bar{t}$ production. Furthermore, the hadronic W peaks provide the most ideal calibration for the jet energy scale of the two experiments. Note that it is extremely difficult to get the scale information from inclusive W decays to two jets, because of the very high QCD di-jet background which would both mask the signal and saturate the data acquisition bandwidth.

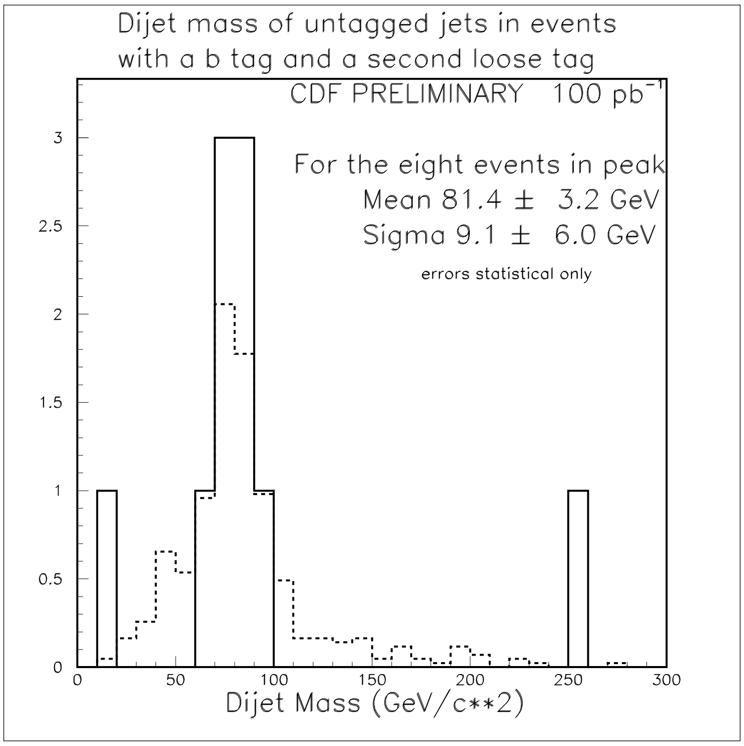

FIG. 106. The di-jet mass of untagged jets in data events with a double b-tag (histogram), compared to the expected signal from the top Monte Carlo (dotted). The integrated luminosity for this data set is 100 pb^{-1}. From the CDF collaboration, Yao, 1995.

The hadronic W has been reconstructed by the CDF collaboration (Yao, 1995). The method uses $W+ \geq 4$ jet events with two b-tagged jets. One of the jets is tagged using either of the standard CDF lepton or vertex tagging algorithms. In order to increase the statistics of the sample, the second jet is tagged using a looser vertex tag algorithm. Such a double-tag requirement considerably reduces many sources of background, and the $t\bar{t}$ purity of the sample is very high. Just as in the constrained fit procedure described in Section IX.A, only the four highest E_T jets are considered. With this restriction, in a doubly b-tagged $t\bar{t}$ event there is no ambiguity in assigning jets to the hadronic W-decay. The invariant mass distribution of the two untagged jets in this sample is shown in Fig. 106. In eight of the ten events, the invariant masses of the two untagged jets cluster tightly around $M_{jj} \approx 80$ GeV/c^2. This provides overwhelming evidence for the presence of hadronic decays of W bosons in the lepton + jets + b-tag sample. The two outlying events are most likely due to cases where one of the untagged jets considered to be from the W is really a gluon jet from initial or final state radiation.

The D0 hadronic W mass reconstruction procedure (Strovink, 1995) in lepton + jets events is much more complicated, since the b-tag in D0 is not as efficient as in CDF. The analysis uses lepton + $\geq$ 4 jets data, and considers only the four jets with the highest E_T. Just as in the constrained fit procedure (see Section IX.A), the neutrino longitudinal momentum ($P_{L\nu}$) is obtained by constraining the lepton-neutrino invariant mass to the W-mass, and only the solution with the smallest $|P_{L\nu}|$ is considered. No constraint is placed on the di-jet mass, so that there are four different ways of partitioning the event into $(l\nu j_1)$ and $(j_2 j_3 j_4)$, unless one of the jets is b-tagged, in which case the number of combinations is two. A two-dimensional scatter-plot of di-jet mass versus top mass is filled for each combination with weight proportional to $\exp(-\chi^2/2)$, where $\chi^2 \equiv \ln^2(\text{mass}(l\nu j_1)/\text{mass}(j_2 j_3 j_4))$. The normalization is chosen in such a way that the weights for all combinations in a given event sum to unity. The top mass is defined as the average of mass$(l\nu j_1)$ and mass$(j_2 j_3 j_4)$ for electron + jets events. For muon + jets events, the top mass is calculated by taking a weighted average of the two, with the values of hadronic and leptonic masses weighted in the ratio 60 : 40. The di-jet mass is defined as follows. If one of the jets in $(j_2 j_3 j_4)$ is tagged, the di-jet mass is the invariant mass of the two other jets. Otherwise, the most energetic jet in the top rest frame is used as the b. But if no jets in $(j_2 j_3 j_4)$ are tagged, and their energy in the top rest frame are such that $(E_2 - E_3) < (E_3 - E_4)$, then the permutation is plotted twice, with equal weights, with di-jet mass chosen as mass$(j_3 j_4)$ or mass$(j_2 j_4)$. Studies of $t\bar{t}$ Monte Carlo events, indicate that this procedure results in a peak in the di-jet-mass vs. top-mass scatter plot at di-jet-mass = M_W and top-mass = M_{top}. On the other hand, background events are expected to peak at lower values. Projections from the di-jet-mass vs. top mass scatter plot are shown in Fig. 107. The top mass and di-jet mass distributions are peaked around 180 and 80 GeV/c^2 respectively. The probability for these distributions to be consistent with the background-only hypothesis is 1.3%.

In conclusion, both collaborations have shown evidence for hadronic W decays in their respective top event samples. With the aid of vertex tagging, the CDF $W \to q\bar{q}$ peak is very clean and straightforward to understand. Future higher statistics samples of $W \to q\bar{q}$ in top events will provide a very important calibration to the top mass measurement, see Section X.

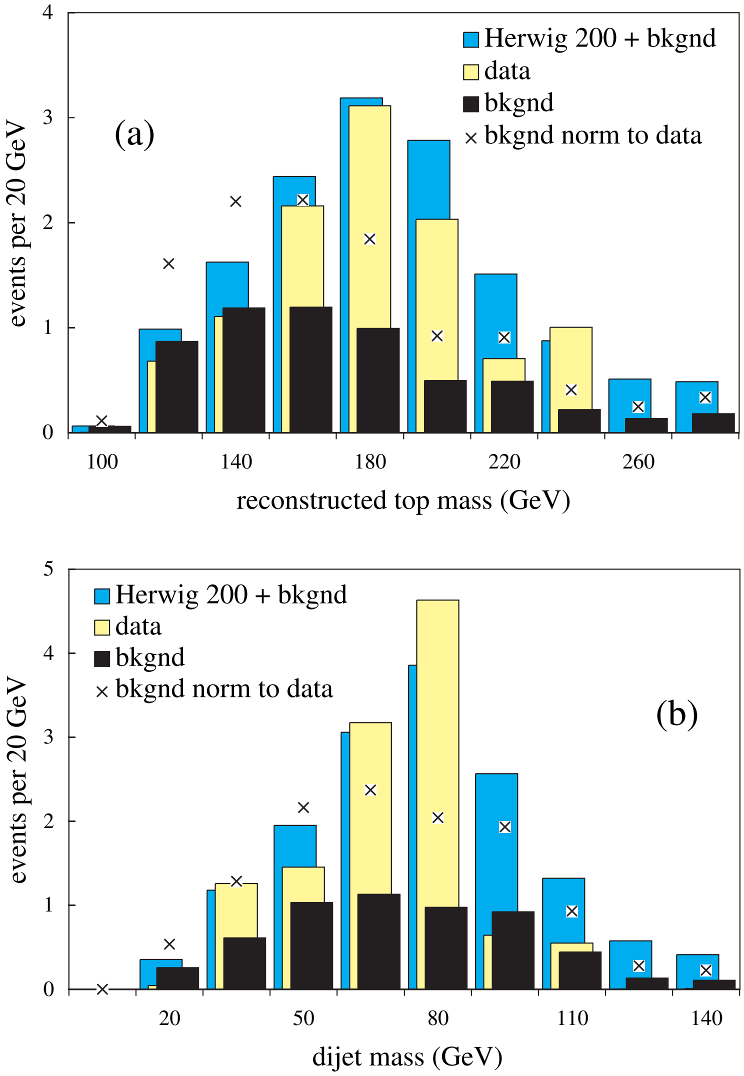

FIG. 107. Distributions of (a) reconstructed top quark mass, and (b) reconstructed di-jet-mass. The reconstructed top-mass is plotted only for di-jet-mass > 58 GeV/c^2. The reconstructed di-jet mass is plotted only for top mass > 150 GeV/c^2. Distributions are shown for data, sum of background and HERWIG $t\bar{t}$ Monte Carlo, background alone, and background normalized to match the area of the data. From the D0 collaboration, Strovink, 1995.

X. FUTURE PROSPECTS

One of the goals of particle physics in the next decade is to perform detailed experimental studies of the properties of the top quark. Since the mass of the top quark is of the same order as the scale for electroweak symmetry breaking, it is possible that new physics effects will manifests themselves in the top sector. While we do not know what these new effects might be, it is clear that top quark physics represents an opportunity to uncover physics beyond the Standard Model.

In this Section we will concentrate on prospects for top physics at the Tevatron. We will begin by briefly summarizing plans for the upgrade of the accelerator and the detectors in Section X.A. Detailed studies of the possibilities for the Tevatron top physics program are well under way (Amidei and Brock, 1996). Prospects for improving the accuracy of the top mass measurement will be discussed in Section X.B; the potential for study of the Wtb vertex will be addressed in Section X.C; finally, additional tests of the Standard Model, as well as searches for new physics involving the top quark will be discussed in Section X.D.

A. Accelerator and detector upgrades

The CDF (CDF collaboration, 1995) and D0 (Tuts, 1996) detectors at the Tevatron will be undergoing major upgrades in the next few years. The most significant improvements for top physics will be the installation of a magnet for charged particle momentum determination in D0 and new 3D silicon vertex detectors in both detectors. Since vertex-tagging of b-quarks in top events has been shown to be such a powerful tool, the capabilities of the upgraded D0 detector for top physics will be considerably enhanced. The new CDF silicon vertex detector will also have a significant impact in the top physics program at CDF. With three dimensional information, the b-tagging efficiency will be improved, and the instrumental background level will be reduced; furthermore, the new vertex detector will be long enough to cover the whole luminous region of the Tevatron, increasing the acceptance for vertex tags (recall that the geometrical coverage of the present CDF vertex detector is only about 60%, see Section VIII.B.3).

At the same time, the Fermilab accelerator complex will be upgraded with the construction of a new high intensity 120 GeV proton accelerator (*The Main Injector*). The Main Injector will replace the Main Ring, whose aperture currently limits the luminosity, as the injector to both the Tevatron and the $\bar{p}$ source. In addition, a new 8 GeV permanent magnet ring (*Recycler*) has been proposed to achieve a more efficient accumulation of antiprotons by recycling (hence the name) the $\bar{p}$ from the previous store, store the anti-protons when the accumulator is full, and protect them from power glitches in the accelerator (Foster, 1995; Jackson, 1995). The number of bunches will also be increased from 6 to 36, allowing higher luminosity without increasing the number of interactions per crossing. This increase shortens the bunch crossing interval from the current value of 3.5 μsec to 396 ns. This requires an upgraded trigger, data acquisition and front-end electronics systems, which must be pipelined to handle the increased rate. After completion of these upgrades in 1998-99, the Tevatron luminosity will be increased by one order of magnitude to 2 x 10^{32} cm^{-2}s^{-1}, with further luminosity improvements likely to occur in the following years. The center-of-mass energy of the Tevatron is also expected to increase from 1.8 TeV to 2 TeV, resulting in a increase of approximately 30% in the $t\bar{t}$ cross-section.

This series of improvements in the Fermilab collider program will allow for much more detailed studies of the top quark than those that are possible with the low statistics data samples that are available now. The projected sizes of the $t\bar{t}$ samples in each experiment for an integrated luminosity of 1 fb^{-1} will be of order 100 events in the dilepton channel and of order 500 events in the lepton + 4 jets channel with one b-tag, with half of these events having both b-jets tagged (Amidei and Brock, 1996).

In addition, towards the middle of the next decade, the Large Hadron Collider (LHC) at CERN will become operational. The LHC is a very high luminosity ($> 10^{34}$ cm^{-2} s^{-1}) pp machine with $\sqrt{s} = 14$ TeV. At this energy, $\sigma(pp \to t\bar{t}) \approx 700$ pb, a factor of 100 higher than $\sigma(p\bar{p} \to t\bar{t})$ at the Tevatron. With the high luminosity and the high cross-section, the LHC can be considered to be a top-factory. In the even more distant future, top physics will also be pursued at a very high energy electron collider (e.g. *The Next Linear Collider*, NLC), assuming that such a machine will be built.

B. Improving the top mass measurement

As was discussed in Section III, the top quark mass is a fundamental parameter of the Standard Model. Its value enters in the calculation of radiative corrections to a large number of electroweak observables. It is therefore very important to measure the top quark mass as accurately as possible to allow for precise tests of the Standard Model.

The best value of M_{top} as obtained from fits to the LEP and SLC measurements, as well as the measurements of the W mass from $p\bar{p}$ experiments and deep inelastic neutrino scattering, is $\mathrm{M}_{top} = 179 \pm 9^{+17}_{-10}$ $\mathrm{GeV/c^2}$ where the second uncertainty comes from varying the Higgs mass between 60 and 1000 $\mathrm{GeV/c^2}$ (see Section III). This is in good agreement with the values reported by the CDF ($\mathrm{M}_{top} = 176 \pm 9$ $\mathrm{GeV/c^2}$) and D0 collaborations ($\mathrm{M}_{top} = 170 \pm 18$ $\mathrm{GeV/c^2}$), see Section IX.

The accuracies of the neutrino measurements and of the LEP and SLC measurements at the Z are not expected to dramatically improve in the coming years. On the other hand, the accuracy in the determination of the W mass will improve by almost one order of magnitude, from the Tevatron experiments as well as from $e^+e^- \to W^+W^-$ at LEP200. Within the Standard Model, radiative corrections to the W propagator (see Fig. 11) result in definite predictions for the W mass as a function of the top and Higgs mass (see Fig. 12). It is therefore very interesting to measure both the W mass and the top mass as precisely as possible.

How accurately can the top mass be measured? Experience from CDF and D0 indicates that the method of choice for measuring the top mass is to perform constrained fits on the b-tagged lepton + jets data sample, see Section IX.A. We can extrapolate the statistical accuracy of a future top mass measurement from the present CDF measurement. This measurement has a statistical uncertainty of 6 $\mathrm{GeV/c^2}$ for an integrated luminosity of 110 pb^{-1}. After the first Main Injector run of the Tevatron, we can expect the integrated luminosity to be of order 1 fb^{-1} per experiment, with a 30% increase in top cross-section from running at the higher center of mass energy of 2 TeV, and a 40% increase in geometrical acceptance from the new CDF vertex detector. Since the statistical uncertainty varies inversely as the square root of the number of events, we can expect a statistical uncertainty of order 1.5 GeV/c^2 from CDF. A similar uncertainty can be expected from the upgraded D0 detector. Systematic effects, which at present are at the level of 7 GeV/c^2, will be the limiting factor in the precision of the top mass determination.

The systematic uncertainties in the top mass measurements have been described in Section IX.A.3. The largest uncertainty is due to the understanding of the jet energy scale, as well as the related issue of additional jets from gluon radiation. At this time, it is not entirely clear what the ultimate precision will be. The dominant component of the energy scale uncertainty is related to the reliability of the extrapolation from jet energies to parton energies, and it is the understanding of the QCD process, rather than the understanding of the detector, which limits the measurement. Higher statistics tests of the understanding of the energy scale will be performed in γ + jet and Z + jet events (see Section IX.A.3, Figs. 101, and 102). The Monte Carlo modeling of gluon radiation will be more precisely checked and/or tuned by examining the energy flow within a jet. There will however remain systematic uncertainties related to the transfer of this calibration from the control samples to the hadronic environment in $t\bar{t}$ events. The ultimate size of these uncertainties is at the moment not well understood.

The additional statistics that will become available will be important to reduce the systematic uncertainty. With enough statistics, the number of lepton + jets events with two b-tagged jets will be sizable, and these events will provide a very important tool for understanding systematic uncertainties in the top mass measurement. In these events, there are no ambiguities in assigning the two jets to the hadronic W decay. The invariant mass of these two jets, which ideally should reconstruct to the W mass, provides an in-situ calibration of $W \to$ jet-jet invariant mass reconstruction. First results from this kind of study are very promising, (see Fig. 106). Besides the energy scale issue, studies of doubly-b-tagged events will provide useful handles on other systematic effects that limit the precision of the top mass measurement. Since mis-tag backgrounds in this data sample are very small, events in the tails of the jet-jet invariant mass distribution will be $t\bar{t}$ events with one jet from gluon radiation and W$Q\bar{Q}$ events. Therefore doubly-b-tagged events will be useful in directly measuring these components of the data set. This will improve the understanding of the top resolution function, which also depends on the number of jets from gluon radiation in the sample. The doubly-b-tagged sample will also allow for a test of the modeling of the $WQ\bar{Q}$ background component, which affects the top mass measurement since the top mass is extracted from a likelihood fit of the data to the sum of $t\bar{t}$ and W background. The number of jet-parton combinations for doubly-b-tagged events is only four, as opposed to twelve combinations that must be considered in the present CDF analysis which only demands one b-tag, see Section IX.A.1. Since statistics are not expected to be the limiting factor, it is possible that a measurement of the top mass using these events will be ultimately more accurate than a measurement based on events with one b-tag. Alternatively, these events can be used to study the effect of wrong combinations. Using these events, it will also become possible to measure the probability for the constrained fit to converge to a combination with a b-tagged jet assigned to a light quark jet.

Further improvements in the understanding of the systematic uncertainties will be possible due to the high statistics $t\bar{t}$ samples that will be available. It will become possible to better quantify the effects of gluon radiation by measuring the relative rates of $t\bar{t} \rightarrow$ dilepton + 2 vs. 3 jets, and $t\bar{t} \rightarrow l+$ 4 vs. 5 jets. The modeling of the $W+$ jets background, which at present is entirely based on the VECBOS Monte Carlo, will be tested using the large sample of $Z+$ jets.

In summary, while the ultimate precision of the top quark mass measurement is not fully known at this time, it is likely that an accuracy of order of a few GeV/c^2 will be achievable. In conjunction with a W mass measurement with a precision of tens of MeV/c^2, this measurement will be sensitive to physics beyond the Standard Model, and will provide useful information on the value of the Higgs mass. In Fig. 108 we show what the M_{top} vs. M_W measurements might look like by the year 2000. If the experimental point in the M_W vs. M_{top} plane was to fall outside the region allowed by the Standard Model, this kind of measurement would provide indirect evidence for physics beyond the Standard Model.

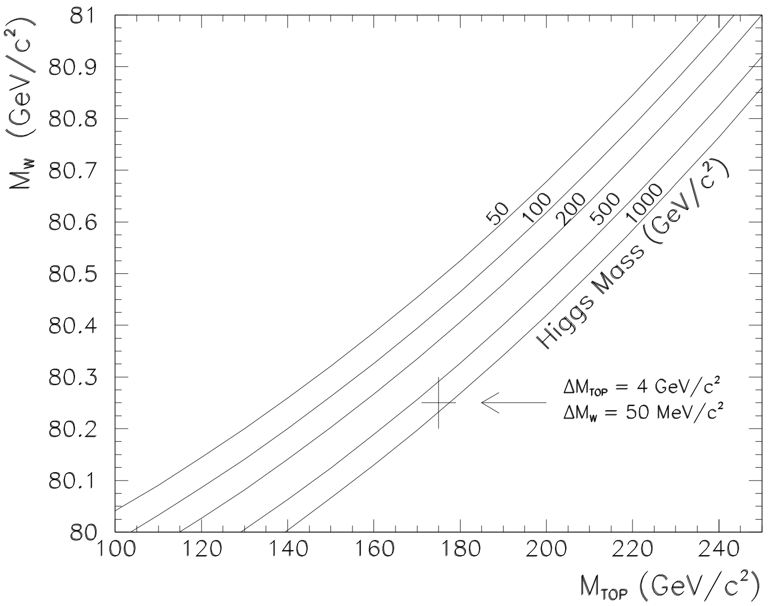

FIG. 108. The expected correlation between the masses of the top, the W and the Higgs. We also show, at an arbitrary point, results of measurements of the W mass to 50 MeV/c^2 and the top mass to 4 GeV/c^2.

C. Probing the Wtb vertex

The structure of the Wtb vertex can be probed by studying top decay and/or production of single top quarks. Up to this point we have mostly discussed $t\bar{t}$ pair production. However, as mentioned in Section IV, top quarks in $p\bar{p}$ collisions can also be produced singly, in the Drell-Yan process $q\bar{q} \rightarrow W^* \rightarrow t\bar{b}$, (see Fig. 17), and in the W-gluon fusion process $qg \rightarrow t\bar{b}q'$, or $qb \to tq'$, (see Fig. 18). The expected cross-sections for Drell-Yan and W-gluon fusion single top production at the Tevatron are displayed in Fig. 21. These cross-sections are smaller than the strong $p\bar{p} \to t\bar{t}$ production cross-section, but they are sizable enough that single top production is expected to be observable at the Tevatron. Production of tW is also allowed, but its cross-section is much smaller.

The potential for studying single top production has attracted a lot of attention for the future top physics program at the Tevatron. The cross-section is proportional to the top quark width, $\Gamma(t \to Wb)$, and within the context of the Standard Model, proportional to the square of the CKM-matrix element $|V_{tb}|$. Note that the top lifetime is too short to be directly measured, (see Fig. 24); furthermore, the top width is very hard if not impossible to measure from the reconstruction of the Breit-Wigner, since the experimental resolution is one order of magnitude worse than the width itself (see Fig. 95). Hence, only indirect measurements of $\Gamma(t \to Wb)$ and $|V_{tb}|$ can be performed.

Assuming three generations and unitarity of the CKM matrix, the value of $|V_{tb}|$ is expected to be very near unity, in the range $0.9988-0.9995$ (Montanet *et al.*, 1994). It is clearly very interesting to test this result. An additional potentially interesting measurement using the single top sample would be a comparison of the rates for $p\bar{p} \to tX$ and $p\bar{p} \to \bar{t}X$, which can be used to search for CP violating effects in the top sector.

The possibility of extracting a single top-quark signal has been examined by many authors (Yuan, 1990; Cortese and Petronzio, 1991; Jikia and Slabospitsky, 1992; Ellis and Parke, 1992; Carlson and Yuan, 1993; Stelzer and Willenbrock, 1995; Amidei and Brock, 1996). Because of the high multi-jet QCD background, only events with $t \to Wb$ followed by $W \to l\nu$ are useful. The signature then is a lepton, missing energy, and two b-jets for Drell-Yan $q\bar{q} \to W^* \to t\bar{b}$ production, and one or two b-jets + one light quark jet for W-gluon fusion, ($qg \to t\bar{b}q'$ or $qb \to tq'$, see Fig. 18). Just as in the $t\bar{t}$ search, the main background is from $W+$ jets production (see Section V.E.1), and b-tagging must be used to reduce this background to a manageable level. Rejection of the tagged $WQ\bar{Q}$ background can be achieved by requiring the mass of the lepton, neutrino, and b-jet to reconstruct to the known top mass. Pair production of $t\bar{t}$ also constitutes a significant background to observation of single top production. Since the jet multiplicity in $t\bar{t}$ events is higher, the optimal sample in which to isolate the single top signal seems to be that of events with one lepton + $\not{E}_{\mathrm{T}}+$ two and only two jets.

A study of the expected signal and background for single top production at the Tevatron shows that a signal-to-background of order 1 to 2 can be achieved. The number of signal events for $|V_{tb}| \approx 1$ would be of order 120 per fb^{-1}, resulting in a statistical uncertainty in the cross-section measurement of order 17% in a 1 fb^{-1} data set (Amidei and Brock, 1996). An additional study, optimized for the detection of the Drell-Yan $q\bar{q} \to W^* \to t\bar{b}$ process, suggests that with the requirement of a double b-tag the signal can be isolated, (see Fig. 109 Stelzer and Willenbrock, 1995). Indications from this study are that, assuming that $|V_{tb}|$ is indeed close to unity, a 3 fb^{-1} exposure would yield a 20% measurement of the cross-section, and therefore a 10% measurement of $|V_{tb}|$. If on the other hand no signal is seen in 3 fb^{-1}, then $|V_{tb}| < 0.60$ at the 95% confidence level. The authors of this study also suggest that the Drell-Yan process may be more useful in extracting $|V_{tb}|$ than the W-gluon fusion process. This is because expectations for the cross-section for $p\bar{p} \to W^* \to t\bar{b}$ are well understood, and can be also normalized to the observed rate of $p\bar{p} \to W^* \to l\nu$. In contrast, the calculation of W-gluon fusion suffers from uncertainties in the higher order corrections as well as in the input gluon density.

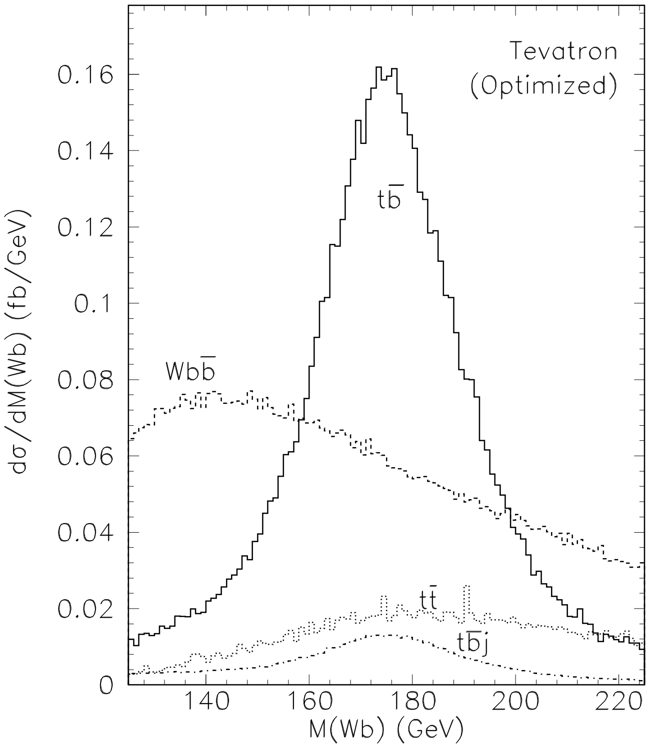

FIG. 109. Expected observed cross-section for $p\bar{p} \to W^* \to t\bar{b}$, $t \to Wb$, $W \to l\nu$ as a function of the invariant mass of the Wb. Also shown are expectations for the most important backgrounds ($t\bar{b}j$ denotes W-gluon fusion). This analysis is based on the $W+$ 2 jets sample. From Stelzer and Willenbrock, 1995.

The CKM matrix element $|V_{tb}|$ can also be measured from the ratio of branching ratios

$$\frac{Br(t \to Wb)}{Br(t \to Wq)} = \frac{|V_{tb}|^2}{|V_{tb}|^2 + |V_{ts}|^2 + |V_{td}|^2}$$

The b-tag can differentiate between $t \to Wb$ and $t \to Wd$ or Ws. Therefore, this ratio can be measured by comparing the number of single- and double-b-tagged $t\bar{t} \to$ lepton + jets events and by measuring the tagging rate in $t\bar{t} \to$ dilepton events. A preliminary analysis by the CDF collaboration finds (Yao, 1995):

$$\frac{Br(t \to Wb)}{Br(t \to Wq)} = 0.94 \pm 0.27 \pm 0.13$$

and sets a (not-yet-very-interesting) limit $|V_{tb}| > 0.022$ at the 95% confidence level. The statistical sensitivity for this branching ratio measurement is projected to be 3% for a 1 fb^{-1} exposure (Amidei and Brock, 1996).

Top decays also provide a unique opportunity to test the the structure of the charged weak current at the $t \to Wb$ vertex. Because the top quark is so heavy, it is possible that new physics may manifest itself at the Wtb vertex. The most general form of the Wtb interaction is (Kane, Ladinsky, and Yuan, 1992) :

$$\begin{aligned} L \;=\; & \frac{g}{\sqrt{2}} \left[W_\mu^- \bar{b} \gamma^\mu (f_1^L P_- + f_1^R P_+) t \;-\; \frac{1}{M_W} \partial_\nu W_\mu^- \bar{b} \sigma^{\mu\nu} (f_2^L P_- + f_2^R P_+) t \right] \;+ \\ & \frac{g}{\sqrt{2}} \left[W_\mu^+ \bar{t} \gamma^\mu (f_1^{L*} P_- + f_1^{R*} P_+) b \;-\; \frac{1}{M_W} \partial_\nu W_\mu^+ \bar{t} \sigma^{\mu\nu} (f_2^{R*} P_- + f_2^{L*} P_+) b \right] \end{aligned}$$

where $P_\pm = \frac{1}{2}(1 \pm \gamma_5)$ and $i\sigma^{\mu\nu} = -\frac{1}{2}[\gamma^\mu, \gamma^\nu]$.

The quantities f_1^L and f_1^R parametrize the strength of the left-handed and right-handed weak charged current. The f_2's can be interpreted as giving rise to an anomalous weak magnetic moment. In the Standard Model at tree level $f_1^L = 1$ and $f_1^R = f_2^L = f_2^R = 0$. There is obviously no direct experimental information on these form factors, although consistency with the measured branching ratio for $b \to s\gamma$ constrains f_1^R to be at most a few percent (Fujikawa and Yamada, 1994).

The polarization of the W in the $t \to Wb$ decay probes the values of the form factors. Denoting the left-handed, right-handed, and longitudinal polarization states of the W by λ_-, λ_+, and λ_0 respectively, the expected relative polarizations of the W boson after averaging over the top and bottom polarization states, are (Kane, Ladinsky, and Yuan, 1992) :

$$\begin{aligned} \lambda_- &= |f_1^L + \beta f_2^R|^2 \\ \lambda_+ &= |f_1^R + \beta f_2^L|^2 \\ \lambda_0 &= \frac{1}{2}|f_2^R + \beta f_1^L|^2 \;+\; \frac{1}{2}|f_2^L + \beta f_1^R|^2 \end{aligned}$$

with $\beta = \frac{M_{top}}{M_W}$. Therefore, the Standard Model predicts $\lambda_+ = 0$, and the fraction of longitudinally polarized W-bosons in top decays is $\frac{1}{2}\beta^2$. These polarizations can be measured from the angle of emission of the lepton in W-decays. Studies indicate that the statistical accuracies in the measurements of λ_0 and λ_+ in an exposure of 1 fb^{-1} at the Tevatron should be 5% and 2% respectively (Amidei and Brock, 1996). These form factors can also be probed by measuring the single top production cross-section (Carlson, Malkawi, and Yuan, 1994; Malkawi and Yuan, 1994).

The longitudinal polarization state of the W is directly connected with the breaking of electroweak symmetry, since it arises from the Goldstone boson degree of freedom. This kind of study therefore provides a rather unique and particularly interesting test of the Standard Model.

The $p\bar{p} \to t\bar{t}$ cross-section can be calculated in QCD. Its measurement tests the predictive power of QCD and is sensitive to new physics. Considerable theoretical interest in the subject was triggered by the initial measurement of the $t\bar{t}$ cross-section by the CDF collaboration (F. Abe *et al.*, 1994a). The measured value was higher than expected, although still consistent with the QCD calculation, within the large experimental uncertainties. The more recent higher statistics measurement by both CDF and D0 are in better agreement with the calculation (see Fig. 92).

The precision of the $t\bar{t}$ cross-section measurement depends on the accuracy of the luminosity normalization (3.5%), the background estimate, and the acceptance calculation. The uncertainty in the acceptance calculation is mostly due to the uncertainty in the b-tag efficiency and the uncertainties in the modeling of $t\bar{t}$ production (e.g. the effects of gluon radiation). The high statistics $t\bar{t}$ data samples that will be collected at the Tevatron will provide several handles to reduce this uncertainty. It is not clear what the ultimate systematic uncertainty on the $t\bar{t}$ cross-section will be; our guess is that a precision of 10%, comparable to the uncertainty in the QCD calculation of $t\bar{t}$ production, should be achievable.

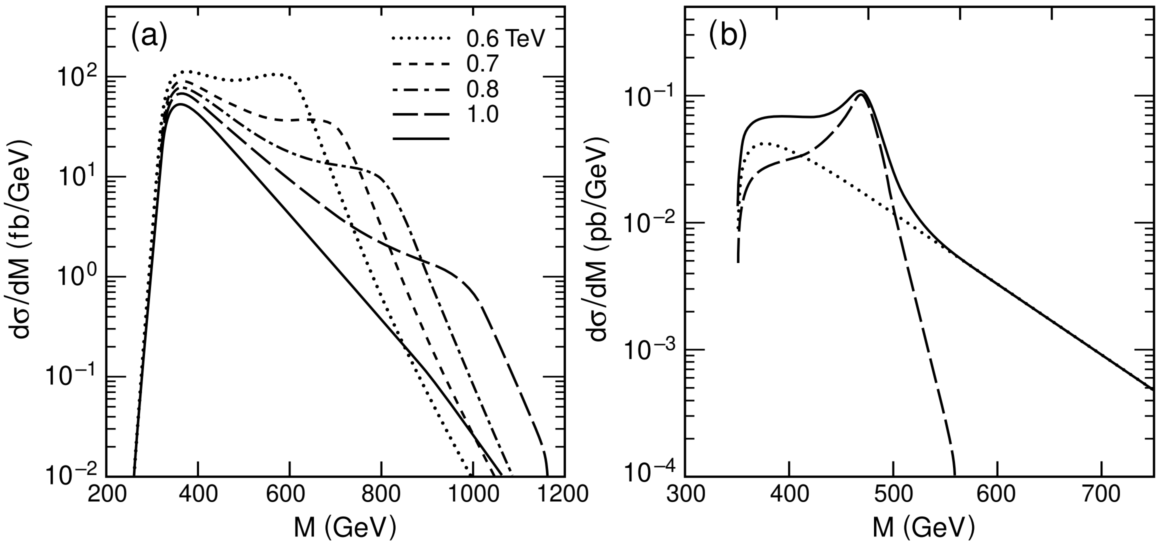

FIG. 110. Expected invariant mass of the $t\bar{t}$ pair : (a) including the contribution of a color octet vector meson in the top color model (from Hill and Parke, 1994). The different curves show the expectation as the vector meson mass varies from 600 GeV/c^2 to infinity. (b) including the effect of a 475 GeV/c^2 color-octet technipion in multiscale walking technicolor (from Lane, 1995). The dotted line is the QCD prediction; the dashed line is the technipion contribution; and the solid line is the sum of the two.

Large enhancements to the $t\bar{t}$ cross-section and, more dramatically, resonances in the $t\bar{t}$ invariant mass spectrum are expected in a number of models, (see Fig. 110). These could be due to color octet vector mesons (Hill and Parke, 1994) in models where the electroweak symmetry breaking is realized via top condensation (Hill, 1991; Martin, 1992a and 1992b), or to technipions (Eichten and Lane, 1994) in multiscale models of walking technicolor (Lane and Eichten, 1989; Lane and Ramana, 1991).

Measurements of the $t\bar{t}$ invariant mass distributions are possible in the lepton + jets channel. Preliminary CDF (Yao, 1995) and D0 (Narain, 1996) analyses are consistent with QCD expectations, (see Fig. 111). With the high statistics that will become available, these models will be critically tested in the future.

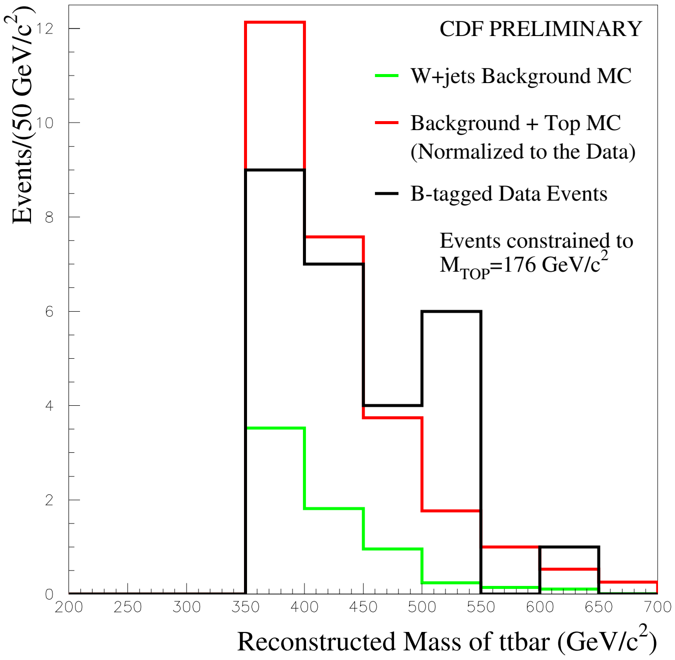

FIG. 111. Reconstructed invariant mass of the $t\bar{t}$ pair compared to the background and $t\bar{t}$ + background expectations. From the CDF collaboration, Yao, 1995. The integrated luminosity is $\approx$ 100 pb^{-1}.

Chromoelectric and chromomagnetic dipole moments of the top quark affect the structure of the $t\bar{t}$-gluon vertex, and hence affect the $t\bar{t}$ production cross-section and $t\bar{t}$ transverse momentum (Atwood, Kagan, and Rizzo, 1994; Rizzo, 1994; Cheung, 1995; Haberl, Nachtmann, and Wilch, 1995). A top-quark chromomagnetic dipole moment can occur in composite and technicolor models, with magnitude of order $\mathrm{M}_{top}^2/\Lambda^2$, where Λ is the characteristic scale for new physics. As can be seen from Fig. 112, the present measurement of the $t\bar{t}$ cross-section is already accurate enough to probe the scale $\Lambda \approx 200$ GeV. A chromoelectric dipole moment would be CP-violating, and could arise from large couplings between top quarks and Higgs bosons in the multi-Higgs doublet model (Atwood, Aeppli, and Soni, 1992; Brandenburg and Ma, 1993; Cheung, 1995; Haberl, Nachtman, and Wilch, 1995).

CP violation effects in $t\bar{t}$ production would manifest themselves in different polarizations for the t and the $\bar{t}$ (Kane, Ladinsky, and Yuan, 1992; Schmidt and Peskin, 1992, Kao, Ladinsky, and Yuan, 1994). Because the top quark lifetime is short, the top decays before hadronization and polarization information is preserved in the $t \to Wb$ decay. Assuming Standard Model Wtb couplings, the polarization of the top quark is then analyzed by the polarization of the W from the top decay. Examples of CP violating observables that can be studied are differences in rates between $t_L\bar{t}_L$ and $t_R\bar{t}_R$, or $t_L\bar{t}_R$ and $t_R\bar{t}_L$, where the subscripts L and R denote left- and right-handed polarizations respectively.

In the single top production process, top quarks are almost 100% longitudinally polarized, since they are produced through the weak interaction (Carlson and Yuan, 1993). Searches

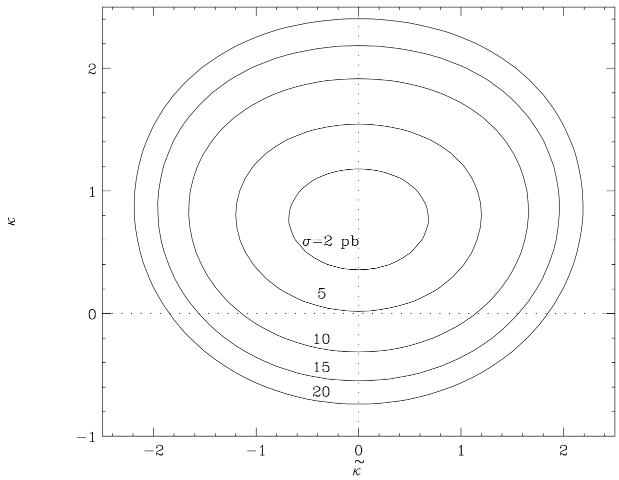

FIG. 112. Contours of $t\bar{t}$ cross-section (M_{top} = 176 GeV/c^2) as a function the chromoelectric ($\tilde{\kappa}$) and chromomagnetic (κ) dipole moments of the top quark.

for CP violation in the top quark decay can then also be carried out in the $t \to W^+ b \to l^+ \nu b$ decay by studying the quantity $\sigma \cdot (\mathbf{P}_b \times \mathbf{P}_l)$, where σ is the top polarization vector (Kane, Ladinsky, and Yuan, 1992; Grzadowski and Gunion, 1992).

Precise measurements of polarization effects in the top sector will however be rather difficult. These measurements require very high statistics and good control of the systematics. Most likely, only very large asymmetries will be accessible experimentally.

Physics beyond the Standard Model can also give rise to exotic decays of the top quark. The measurement of the ratio of branching ratios

$$R = \frac{Br(t\bar{t} \to l + jets)}{Br(t\bar{t} \to ll + jets)}$$

is quite generally sensitive to decays different from $t \to WX$, provided that the new top quark decay mode includes jets. More model-dependent searches for new top quark decays can also be carried out.

One example of a non-Standard Model decay of the top quark is the decay $t \to H^+ b$, which can occur in models with two Higgs doublets, see Sec VI.C. The H$^+$ would then decay into the heaviest fermion pairs, $c\bar{s}$ or $\tau\nu$. The branching ratios depend on the ratio of vacuum expectation values for the two doublets, tanβ, (see Fig. 113). If tanβ is large, the signature for this decay mode would be an excess of lepton + hadronic τ + b-tag events; if tanβ is small, one could search for the $H^+ \to c\bar{s}$ peak in the invariant mass distribution of lepton + jets events. Other possible exotic decays of the top quark which can be searched for include flavor changing neutral current decays such as $t \to Zc$ (Han, Peccei, and Zhuang, 1995) and $t \to \gamma c$, and decays into a supersymmetric top quark (*stop*) and a neutralino (Mrenna and Yuan, 1995). Some preliminary limits on these FCNC have been presented by CDF (LeCompte, 1995).

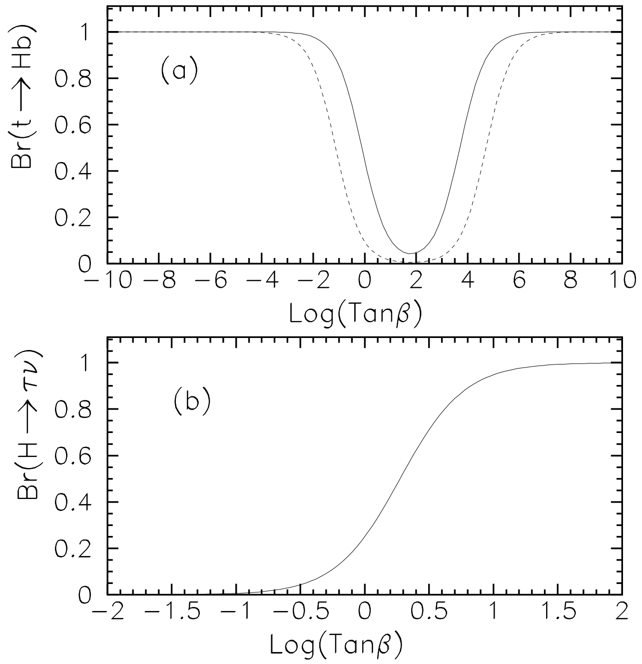

FIG. 113. (a) Expected branching ratios of $t \to H^+b$ in the two Higgs model for M_{top} = 180 GeV/c^2 as a function of log(tanβ). Solid line: M_H = 70 GeV/c^2; dashed line: M_H = 150 GeV/c^2. (b) Expected branching ratio for $H^+ \to \tau\nu$ as a function of log(tanβ).

XI. CONCLUSION

The evidence for the existence of the top quark from the CDF and D0 collaborations at the Tevatron is persuasive. The mass of the top quark is M_{top} = 175 ± 8 GeV/c^2, in agreement with expectations from precision electroweak measurements. This mass is a factor of forty higher than the mass of the second heaviest fundamental fermion, and is of the same order of magnitude as the scale for electroweak symmetry breaking. The high mass of the top quark is a somewhat of a surprise; in Fig. 114 we show the evolution of the top mass limits and measurements since the discovery of the companion b-quark. It is interesting to notice that theoretical arguments based on local supersymmetry from the early eighties, when the experimental lower limit on the top quark mass was only approximately 20 GeV/c^2, favored a rather high top mass, see Section II. It is however still far from clear whether the high value of the top mass is an accident, or a consequence of physics at a higher mass scale.

The properties of the top quark will be studied much more precisely at the upgraded Tevatron starting in 1999. There is a possibility that effects beyond the Standard Model will manifest themselves in the top sector. If that is the case, the CDF and D0 collaborations are well positioned to observe them. In the more distant future, the LHC pp collider at CERN, with the higher energy and luminosity, will serve as a $t\bar{t}$ factory.

ACKNOWLEDGMENTS

First of all, we wish to thank our CDF colleagues with whom we shared the excitement of the hunt for the top quark. A number of people helped us to write this review. N. Hadley,

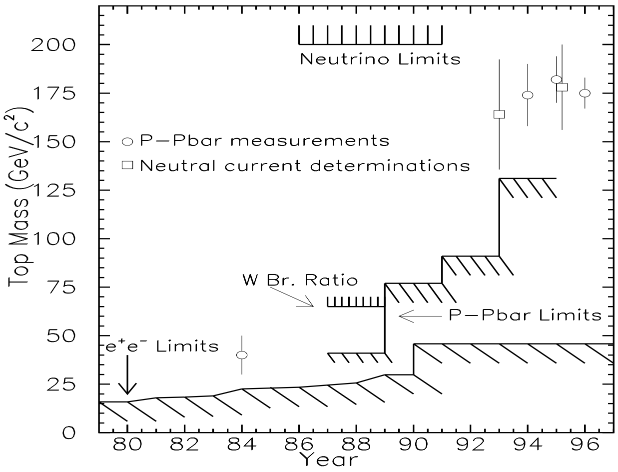

FIG. 114. A brief history of the search for the top quark. Here we show the limits from searches in e^+e^- (Section VI.A) and $p\bar{p}$ (Section VI.B). The square data points are predictions from neutral current studies, mostly at LEP and SLC (Section III). We also show the limit from neutrino experiments that were obtained prior to the commissioning of LEP and SLC (Amaldi *et al.*, 1987). The circular data points show the recent measurements of the top mass (Section IX.A), as well as the UA1 1984 result $M_{top} = 40 \pm 10$ GeV/c^2, which turned out to be wrong (Section VI.B). Just for fun, we also show the **upper** limit on the top mass from early measurements of the W leptonic branching ratio at the S$p\bar{p}$S (Section VI.C). More recent measurements of this quantity at both the Tevatron and the S$p\bar{p}$S are consistent with a high top quark mass.

B. Klima, M. Narain, S. Protopopescu, and S. Snyder explained many aspects of the D0 top analysis. E. Laenen kindly provided us with a modern calculation of the $t\bar{t}$ cross-section at S$p\bar{p}$S energies. A. Blondel helped us understand the implications of the very precise neutral current measurements. We also benefited from discussions with D. Amidei, P. Giromini, A. Heinson, S. Holmes, D. Kestenbaum, Y.K.Kim, J. Konigsberg, J. Kroll, M. Kruse, M. Mangano, M. Mannelli, and J. Polchinski. We also wish to thank D. Ceder and D. McLaren for assistance in the preparation of the manuscript.

REFERENCES

Abachi, S. *et al.*, 1994, Phys. Rev. Lett. **72**, 2138.
Abachi, S. *et al.*, 1995a, Phys. Rev. Lett. **74**, 2422.
Abachi, S. *et al.*, 1995b, Phys. Rev. Lett. **74**, 2632.
Abachi, S. *et al.*, 1995c, Phys. Rev. Lett. **75**, 3226.
Abachi, S. *et al.*, 1995d, Phys. Rev. D **52**, 4877.
Abachi, S. *et al.*, 1995e, Phys. Rev. Lett. **75**, 1456.
Abe, F. *et al.*, 1990a, Phys. Rev. Lett. **64**, 142.
Abe, F. *et al.*, 1990b, Phys. Rev. Lett. **64**, 147.
Abe, F. *et al.*, 1990c, Phys. Rev. Lett. **64**, 152.
Abe, F. *et al.*, 1990d, Phys. Rev. Lett. **64**, 348.
Abe, F. *et al.*, 1990e, Phys. Rev. D **41**, 2330.
Abe, F. *et al.*, 1991a, Phys. Rev. D **43**, 664.
Abe, F. *et al.*, 1991b, Phys. Rev. D **44**, 29.
Abe, F. *et al.*, 1991c, Phys. Rev. D **44**, 601.
Abe, F. *et al.*, 1992a, Phys. Rev. Lett. **68**, 447; Phys. Rev. D **45**, 3921.
Abe, F. *et al.*, 1992b, Phys. Rev. Lett. **68**, 3398.
Abe, F. *et al.*, 1992c, Phys. Rev. Lett. **69**, 28.
Abe, F. *et al.*, 1992d, Phys. Rev. D **45**, 1448.
Abe, F. *et al.*, 1993a, Phys. Rev. Lett. **70**, 713.
Abe, F. *et al.*, 1993b, Phys. Rev. Lett. **70**, 4042.
Abe, F. *et al.*, 1993c, Phys. Rev. D **47**, 4587.
Abe, F. *et al.*, 1993d, Phys. Rev. Lett. **71**, 3421.
Abe, F. *et al.*, 1994a, Phys. Rev. D **50**, 2966; Phys. Rev. Lett. **73**, 225.
Abe, F. *et al.*, 1994b, Phys. Rev. D **50**, 5550.
Abe, F. *et al.*, 1994c, Phys. Rev. Lett. **72**, 1977.
Abe, F. *et al.*, 1994d, Phys. Rev. Lett. **73**, 220.
Abe, F. *et al.*, 1994e, Phys. Rev. Lett. **73**, 2667.
Abe, F. *et al.*, 1995a, Phys. Rev. Lett. **74**, 2662.
Abe, F. *et al.*, 1995b, Phys. Rev. D **51**, 4623; Phys. Rev. Lett. **75**, 1012.
Abe, F. *et al.*, 1995c, Phys. Rev. D **52**, 2605.
Abe, K. *et al.*, 1990, Phys. Lett. B **234**, 382.
Abrams, G.S. *et al.*, 1989, Phys. Rev. Lett. **63**, 2447.
Abramowicz, H. *et al.*, 1986, Phys. Rev. Lett. **57**, 298.
Abreu, P. *et al.*, 1990a, Phys. Lett. B **241**, 449.
Abreu, P. *et al.*, 1990b, Phys. Lett. B **242**, 536.
Abreu, P. *et al.*, 1991, Nucl. Phys. B **2367**, 511.
Adachi, I. *et al.*, 1988, Phys. Rev. Lett. **60**, 97.
Adeva, B. *et al.*, 1983a, Phys. Rev. Lett. **50**, 799.
Adeva, B. *et al.*, 1983b, Phys. Rev. Lett. **51**, 443.
Adeva, B. *et al.*, 1985, Phys. Lett. B **152**, 439.
Adeva, B. *et al.*, 1986, Phys. Rev. D **34**, 681.
Adriani, O. *et al.*, 1992, Phys. Lett. B **294**, 457.
Adriani, O. *et al.*, 1993, Phys. Rep. **236**, 1.

Agrawal, P. and S.D. Ellis, 1989, Phys. Lett. B **221**, 393.
Akers, R. *et al.*, 1995, Phys. Lett. B **353**, 595.
Akesson, T. *et al.*, 1990, Z. Phys. C **46**, 179.
Akrawi, M.Z. *et al.*, 1990a, Phys. Lett. B **236**, 364.
Akrawi, M.Z. *et al.*, 1990b, Phys. Lett. B **242**, 299.
Albajar, C. *et al.*, 1987, Phys. Lett. B **198**, 271.
Albajar, C. *et al.*, 1988, Z. Phys. C **37**, 505.
Albajar, C. *et al.*, 1989, Z. Phys. C **44**, 15.
Albajar, C. *et al.*, 1990, Z. Phys. C **48**, 1.
Albajar, C. *et al.*, 1991a, Phys. Lett. B **253**, 503.
Albajar, C. *et al.*, 1991b, Phys. Lett. B **257**, 459.
Allaby, J.V., *et al.*, 1986, Phys. Lett. B **177**,446.
Allaby, J.V., *et al.*, 1987, Z. Phys. C **36**, 611.
Alitti, J. *et al.*, 1990a, Z. Phys. C **47**, 11.
Alitti, J. *et al.*, 1990b, Phys. Lett. B **235**, 363.
Alitti, J. *et al.*, 1991a, Z. Phys. C **49**, 17.
Alitti, J. *et al.*, 1991b, Z. Phys. C **52**, 209.
Alitti, J. *et al.*, 1991c, Phys. Lett. B **263**, 563.
Alitti, J. *et al.*, 1992a, Phys. Lett. B **276**, 354.
Alitti, J. *et al.*, 1992b, Phys. Lett. B **276**, 365.
Alitti, J. *et al.*, 1992c, Phys. Lett. B **280**, 365.
Altarelli, G. *et al.*, 1988, Nucl. Phys. B **308**, 724.
Altarelli, G., R. Kleiss, and C. Verzegnassi (editors), 1989, *Z Physics at LEP 1, Volume 1*, CERN-89-08.
Altarelli, G., *et al.*, 1996, CERN Preprint CERN-TH-96-20.
Althoff, M. *et al.*, 1984a, Z. Phys. C **22**, 307.
Althoff, M. *et al.*, 1984b, Phys. Lett. B **138**, 441.
Alvarez-Gaume, L., J. Polchinski, and M.B. Wise, 1983, Nucl. Phys. B **221**, 495.
Amaldi, U., *et al.*, 1987, Phys. Rev. D **36**, 1385.
Amidei, D. *et al.*, 1994, Nucl. Inst. and Meth. A **350**, 73.
Amidei, D. and C. Brock (editors), 1996, *Report of the Tev 2000 Working Group*, Fermilab Preprint Fermilab-Pub-96/082.
Ansari, R. *et al.*, 1987, Phys. Lett. B **194**, 158.
Anselmo, F., B. van Eijk, and G. Bordes, 1992, Phys. Rev. D **45**, 2312.
Arnison, G. *et al.*, 1984, Phys. Lett. B **147**, 493.
Arroyo, C.G., *et al.*, 1994, Phys. Rev. Lett. **72**, 3452.
Atwood, D., A. Aeppli, and A. Soni, 1992, Phys. Rev. Lett. **69**, 2754.
Atwood, D., A. Kagan, and T.G. Rizzo, 1995, Phys. Rev. D **52**, 6264.
Azzi, P. *et al.*, 1995, Nucl. Instrum. Meth. A **360**, 137.
Babcock, J., D. Sivers, and S. Wolfram, 1978, Phys. Rev. D **18**, 162.
Baer, H., V. Barger, and R.J.N. Phillips, 1989, Phys. Rev. D **39**, 2809 and 3953.
Baer, H. *et al.*, 1990, Phys. Rev. D **42**, 54.
Barber, D.P. *et al.*, 1979, Phys. Lett. B **85**, 463.
Barber, D.P. *et al.*, 1980, Phys. Rev. Lett. **44**, 1722.
Barger, V., J.L. Hewett, and R.J.N. Phillips, 1990, Phys. Rev. D **41**, 3421.

Barger, V., J. Ohnemus, and R.J.N. Phillips, 1993, Phys. Rev. D **48**, 3953.
Barger, V. *et al.*, 1994, Phys. Lett. B **338**, 336.
Barger, V. *et al.*, 1995, Phys. Lett. B **344**, 329.
Barger, V. and R. Phillips, 1987, in *Collider Physics*, (Addison-Wesley, Redwood City, Ca) p. 259.
Bartel, W. *et al.*, 1979a, Phys. Lett. B **88**, 171.
Bartel, W. *et al.*, 1979b, Phys. Lett. B **89**, 136.
Bartel, W. *et al.*, 1981, Phys. Lett. B **99**, 277.
Bartel, W. *et al.*, 1984, Phys. Lett. B **146**, 437.
Beenaker, W. *et al.*, 1991, Nucl. Phys. B **351**, 507.
Behrend, H.J. *et al.*, 1984, Phys. Lett. B **144**, 297.
Benlloch, J.M., N. Wainer, and W.T. Giele, 1993, Phys. Rev. D **48**, 5226.
Benlloch, J.M., K. Sumorok, and W.T. Giele, 1994, Nucl. Phys. B **425**, 3.
Berends, F.A., W.T. Giele, and H. Kuijf, 1989, Nucl. Phys. B **321**, 39.
Berends, F.A. *et al.*, 1989, Phys. Lett. B **224**, 237.
Berends, F.A. *et al.*, 1991, Nucl. Phys. B **357**, 32.
Berends, F.A., J.B. Tausk, and W.T. Giele, 1993, Phys. Rev. D **47**, 2746.
Berger, Ch. *et al.*, 1978, Phys. Lett. B **76**, 243.
Berger, Ch. *et al.*, 1979, Phys. Lett. B **86**, 413.
Berger, Ch. *et al.*, 1980, Phys. Rev. Lett. **45**, 1533.
Berger, E.L. *et al.*, 1989, Phys. Rev. D **40**, 83.
Berger, E. L. and H. Contopanagos, 1995, Phys. Lett. B **361**, 115.
Bethke, S., 1995, Nucl. Phys. B (Proc. Suppl.), **39B,C** 198.
Bienlein, J.K. *et al.*, 1978, Phys. Lett. B **78**, 360.
Bigi, I. *et al.*, 1986, Phys. Lett. B **181**, 157.
Blondel, A. *et al.*, 1990, Z. Phys. C **45**, 361.
Bordes, G. and B. van Eijk, 1993, Z. Phys. C **57**, 81.
Bordes, G. and B. van Eijk, 1995, Nucl. Phys. B **435**, 23.
Brandelik, R. *et al.*, 1982, Phys. Lett. B **113**, 499.
Brandenburg, A. and J.P. Ma, 1993, Phys. Lett. B **298**, 211.
Büchmuller, W., G. Grunberg, and S.H.H. Tye, 1980, Phys. Rev. Lett. **45**, 103; *Erratum:* ibid. **45**, 587 (1980).
Buskulic, D. *et al.*, 1992, Phys. Rep. **216**, 253.
Cabibbo, N. 1983, in *Proceedings of the 3rd topical workshop on proton-antiproton collider physics, Rome, Italy, 12-14 January 1983*, edited by C. Bacci and G. Salvini (European Organization for Nuclear Research, Geneva) p. 567.
Carithers, W. 1995, Fermilab seminar 3/2/1995.
Carlson, D.O., E. Malkawi, and C.P. Yuan, 1994, Phys. Lett. B **337**, 145.
Carlson, D.O. and C.P. Yuan, 1993, Phys. Lett. B **306**, 386.
Carlson, D.O. and C.P. Yuan, 1995, Michigan State University Preprint MSUHEP-50823.
Castro, A., 1994, Fermilab Preprint Fermilab-CONF-94/152-E.
Catani, S. *et al.*, 1996, CERN Preprint CERN-TH/96-21.
CDF Collaboration, 1995, *The CDF upgrade*, CDF note CDF/DOC/CDF/PUBLIC/3171.
Cheung, K., 1996, Phys. Rev. D **53**, 3604.
Church, M.D. and J. P. Marriner, 1993, Annu. Rev. Nucl. Part. Sci. **43**, 253.

Cobal, M., H. Grassmann, and S. Leone, 1994, Nuovo Cimento A **107**, 75.

Colas, P., D. Denegri, and C. Stubenrauch, 1988, Z. Phys. C **40**, 527.

Collins, J.C., D.E. Soper, and G. Sterman, 1986 Nucl. Phys. B **263**, 37.

Combridge, B.L., 1979, Nucl. Phys. B **151**, 429.

Contopanagos, H. and G. Sterman, 1993, Nucl. Phys. B **400**, 211.

Contopanagos, H. and G. Sterman, 1994, Nucl. Phys. B **419**, 77.

Cortese S. and R. Petronzio, 1991, Phys. Lett. B **253**, 494.

Dalitz, R.K. and G. Goldstein, 1992, Phys. Rev. D **45**, 1531.

Darden, C.W. *et al.*, 1978, Phys. Lett. B **76**, 246.

Decamp, D. *et al.*, 1990, Phys. Lett. B **236**, 511.

Demortier, L., 1991, PhD thesis, Brandeis University.

Deshpande, N.G. *et al.*, 1985, Phys. Rev. Lett. **54**, 1757.

Dress, M. and D.P. Roy, 1991, Phys. Lett. B **269**, 155.

Eichten, E. and K. Gottfried, 1977, Phys. Lett. B **66**, 286.

Eichten, E. and K. Lane, 1994, Phys. Lett. B **327**, 129.

Eichten, E. *et al.*, 1984, Rev. Mod. Phys. **56**, 579; *Erratum:* ibid. **58**, 1065 (1986).

Ellis, J. *et al.*, 1983, Phys. Lett. B **125**, 275.

Ellis, R.K. and R.J. Gonsalves, 1985, in *Supercollider Physics, Proceedings of the Oregon Workshop, Eugene, Oregon, 1985*, edited by D. Soper (World Scientific, Singapore), p. 287.

Ellis, R.K., 1991, Phys. Lett. B **259**, 492.

Ellis, R.K. and S. Parke, 1992, Phys. Rev. D **46**, 3785.

Ellis, S.D., R. Kleiss, and W.J. Stirling, 1985, Phys. Lett. B **154**, 435.

Fermilab, 1984, *Design Report for the Tevatron I Project.*

Field, R. and R. Feynman, 1978, Nucl. Phys. B **136**, 1.

Flattum, E., 1996, to be published in *Proceedings of the 11th Topical Workshop on Proton-Antiproton Collider Physics, Padova, Italy.*

Foster, G.W., 1995, in *10th Topical Workshop on Proton-Antiproton Collider Physics*, edited by R. Raja and J. Yoh (American Institute of Physics, Woodbury, NY) p. 201.

Frisch, H.J., 1995, in *95 Electroweak Interactions and Unified Theories*, edited by J. Tran Thanh Van (Editions Frontieres, Gif-sur-Yvette, Cedex-France) p. 69.

Frixione *et al.*, 1995, Phys. Lett. B **351**, 555.

Fujikawa, K. and A. Yamada, 1994, Phys. Rev. D **49**, 5890.

Georgi, H. *et al.*, 1978, Ann. Phys. **114**, 273.

Gerdes, D., 1995, in *Proceedings of Les Rencontres de Physique de la Vallée d'Aoste*, edited by M. Greco (Frascati Physics Series, Frascati, Italy) p. 713.

Giele, W.T., E.W.N. Glover, and D.A. Kosower, 1993, Nucl. Phys. B **403**, 633.

Giele, W.T. and W.J. Stirling, 1990, Nucl. Phys. B **343**, 14.

Glashow, S.L. and E.E. Jenkins, 1987, Phys. Lett. B **196**, 233.

Gluck, M., J.F. Owens, and E. Reya, 1987, Phys. Rev. D **17**, 2324.

Goldstein, G.R., K. Sliwa, and R.H. Dalitz, 1993, Phys. Rev. D **47**, 967.

Grzadowski, B. and J.F. Gunion, 1992, Phys. Lett. B **287**, 237.

Grannis, P., 1995, Fermilab seminar 3/2/1995

Gunion, J.F. and Z. Kunstz, 1985, Phys. Lett. B **161**, 333.

Gunion, J.F. *et al.*, 1990, *The Higgs Hunter's Guide*, Addisson-Wesley, New York.

Haberl, P., O. Nachtmann, and A. Wilch, 1996, Phys. Rev. D **53** 4875.

Hagiwara, K. and T. Yoshino, 1979, Phys. Lett. B **80**, 282.
Hagiwara, K. and D. Zeppenfeld, 1989, Nucl. Phys. B **313**, 560.
Halzen, F., C.S. Kim, and S. Willenbrock, 1988, Phys. Rev. D **37**, 229.
Halzen, F. and M. Marsula, 1983, Phys. Rev. Lett. **51**, 857.
Hamberg, R., W.L. van Neerven, and T. Matsuura, 1991, Nucl. Phys. B **359**, 343.
Han, T., R.D. Peccei, and X. Zhuang, 1995, Nucl. Phys. B **454**, 527.
Heinson, A.P., A.S. Belyaev, and E.E. Boos, 1995, University of California at Riverside preprint UCR-95-17.
Herb, S.W. *et al.*, 1977, Phys. Rev. Lett. **39**, 252.
Hikasa, K., 1984, Phys, Rev. D **29**, 1939.
Hill, C.T., 1991, Phys. Lett. B **266**, 419.
Hill, C.T. and S. Parke, 1994, Phys. Rev. D **49**, 4454.
Ibanez, L. E. and C. Lopez, 1983, Phys. Lett. B **126**, 54.
Igarashi, S. *et al.*, 1988, Phys. Rev. Lett. **60**, 2359.
Ikeda, M., 1990, in *Proceedings of the 8th Topical Workshop on Proton-Antiproton Physics, Castiglione della Pescaia, Italy*, edited by G. Bellettini and A. Scribano (World Scientific, Singapore) p. 558.
Jackson, G, (editor), 1995, *Recycler Ring Conceptual Design Study*, Fermilab Library FERMILAB-TM-1936.
Jikia, G.V. and S.R. Slabospitski, 1992, Phys. Lett. B **295**, 136.
Jones, L.M. and H. Wyld, 1978, Phys. Rev. D **17**, 782.
Kane, G.L., G.A. Ladinsky, and C.P. Yuan, 1992, Phys. Rev. D **45**, 124.
Kane, G.L., and M.E. Peskin, 1982, Nucl. Phys. B **195**, 29.
Kao, C., G.A. Ladinsky, and C.P. Yuan, 1994, in *The Albuquerque Meeting : Proceedings of the 8th Meeting, Division of Particle and Fields of the American Physical Society*, edited by S. Seidel (World Scientific, Singapore) p. 713.
Kestenbaum, D., 1996, PhD thesis, Harvard University.
Kidionakis N. and J. Smith, 1995, Phys. Rev. D **51**, 6092.
Klima, B., 1996, personal communication.
Kleiss, R. and W.J. Stirling, 1985, Nucl. Phys. B **262**, 235.
Kondo, K., 1988, J. Phys. Soc. Jpn **57**, 4126.
Kondo, K., 1991, J. Phys. Soc. Jpn **60**, 836.
Krasemann, K.H. and S. Ono, 1979, Nucl. Phys. B **154**, 283.
Laenen, E., J. Smith, and W.L. van Neerven, 1992, Nucl. Phys. B **369**, 543.
Laenen, E., J. Smith, and W.L. van Neerven, 1994, Phys. Lett. B **321**, 254.
Lane, K., 1995, Phys. Rev. D **52**, 1546.
Lane, K. and E. Eichten, 1989, Phys. Lett. B **222**, 274.
Lane, K. and M.V. Ramana, 1991, Phys. Rev. D **44**, 2678.
Leader, E. and E. Predazzi, 1982, in *An Introduction To Gauge Theories And The New Physics*, (Cambridge University Press, Cambridge, UK) p.76.
LeCompte, T., 1995, to appear in *Proceedings of the 1995 Recontres de Physique de Vietnam.*
Lindgren, M. *et al.*, 1992, Phys. Rev. D **45**, 3038.
Linneman, J.T., 1995, in *Proceedings of the XXVII International Conference on High Energy Physics, 20-27 July 1994, Glasgow, Scotland, UK*, edited by P.J. Bussey and I.G. Knowles (Institute of Physics, Philadelphia, Pa.), p. 823.

Malkawi, E. and C.P. Yuan, 1994, Phys. Rev. D **50**, 4462.
Mangano, M.L., 1993, Nucl. Phys. B **405**, 536.
Mangano, M.L. and P. Nason, 1992, Phys. Lett. B **285**, 160.
Mangano, M.L., P. Nason, and G. Ridolfi, 1992, Nucl. Phys. B **373**, 295.
Marchesini, G. and B.R. Webber, 1984, Nucl. Phys. B **238**, 1.
Marchesini, G. and B.R. Webber, 1988, Nucl. Phys. B **310**, 461.
Martin, A.D., R.G. Roberts, and W.J. Stirling, 1987, Phys. Lett. B **189**, 220.
Martin, A.D., R.G. Roberts, and W.J. Stirling, 1989, Phys. Lett. B **228**, 149.
Martin, S.P., 1992a, Phys. Rev. D **45**, 4283.
Martin, S.P., 1992b, Phys. Rev. D **46**, 2197.
Matteuzzi, C. *et al.*, 1983, Phys. Lett. B **129**, 141.
Montanet, L. *et al.*, 1994, *Review of Particle Properties*, Phys. Rev. D **50**, 1433.
Morfin, J. and W.K. Tung, 1991, Z. Phys. C **53**, 13.
Mrenna, S. and C.P. Yuan, 1996, Phys. Lett. B **367**, 188.
Müller, A.H. and P. Nason, 1985, Phys. Lett. B **157**, 226.
Müller, A.H. and P. Nason, 1986, Nucl. Phys. B **266**, 265.
Narain, M., 1995, personal communication.
Narain, M., 1996, to be published in *Proceedings of the 1996 Les Rencontres de Physique de la Vallée d'Aoste*, edited by M. Greco.
Nason, P., S. Dawson, and R.K. Ellis, 1988, Nucl. Phys. B **303**, 607.
Ohnemus, J., 1991a, Phys. Rev. D **44**, 1403.
Ohnemus, J., 1991b, Phys. Rev. D **44**, 3477.
Ohnemus, J. and J.F. Owens, 1991, Phys. Rev. D **43**, 3626.
Orr, L.H., , 1991, Phys. Rev. D **44**, 88.
Orr, L.H., T. Stelzer, and W.J. Stirling, 1995, Phys. Rev. D **52**, 124.
Paige, F. and S.D. Protopopescu, 1986, Brookhaven National Laboratory Preprint BNL-38034.
Para, A., 1988, in *7th Topical Workshop on Proton-Antiproton Collider Physics*, edited by R. Raja, A. Tollestrup, and J. Yoh (World Scientific, Singapore), p. 131.
Perl, M.L. *et al.*, 1975, Phys. Rev. Lett. **35**, 1489.
Peterson, C. *et al.*, 1983, Phys. Rev. D **17**, 105.
Quigg, C. and J.L. Rosner, 1977, Phys. Lett. B **71**, 153.
Revol, J.P., 1985, in *Proceedings of the 6th workshop on grand unification*, edited by S. Rudaz and T.F. Walsh (World Scientific, Singapore), p. 275.
Rice, E. *et al.*, 1982, Phys. Rev. Lett. **48**, 906.
Rizzo, T.G., 1994, Phys. Rev. D **50**, 4478.
Roser, R., 1995, *10th Topical Workshop on Proton-Antiproton Collider Physics*, edited by R. Raja and J. Yoh (American Institute of Physics, Woodbury, NY) p. 248.
Rosner, J.L., 1989, Phys. Rev. D **39**, 3297; *Erratum:* Phys. Rev. D **40**, 1701 (1989).
Rosner, J.L., C. Quigg, and H.B. Thacker, 1978, Phys. Lett. B **74**, 350.
Sagawa, H. *et al.*, 1988, Phys. Rev. Lett. **60**, 93.
Schmidt, C.R. and M.E. Peskin, 1992, Phys. Rev. Lett. **69**, 410.
Sjöstrand, T. and M. Bengtsson, 1987, Comp. Phys. Comm. **43**, 367.
Snyder, S.S., 1995a, PhD thesis, SUNY-Stony Brook.
Snyder, S.S., 1995b, to appear in *Proceedings of the 1995 International Europhysics Confer-*

ence on High Energy Physics, Brussels, Belgium. Fermilab Preprint Fermilab-PUB-95/341-E

Stelzer, T. and S. Willenbrock, 1995, Phys. Lett. B **357**, 125.

Strovink, M., 1995 to in *10th Topical Workshop on Proton-Antiproton Collider Physics*, edited by R. Raja and J. Yoh (American Institute of Physics, Woodbury, NY) p. 320.

Tartarelli, G.F., 1996, to be published in *Proceedings of the XXXIst Rencontres de Moriond, Electroweak Interactions and Unified Theories*; Fermilab preprint FERMILAB-CONF-96/099-E.

The LEP Collaborations ALEPH,DELPHI,L3,OPAL and the LEP Electroweak Working Group, 1995, CERN Preprint CERN-PPE/95-172.

Thompson, W.J., 1994, PhD thesis, SUNY-Stony Brook.

Tuts, P.M., 1996, in *Proceedings of the International Europhysics Conference on High-Energy Physics*, edited by J. Lemonne, C. Vander Velde, and F. Verbeure (World Scientific, Singapore), p. 187.

van der Meer, S., 1972, CERN Internal Report, CERN/ISR-PO/72-31.

van Neerven, W.L. and E.B. Zijlstra, 1992, Nucl Phys. B **382**, 11.

Voloshin, M. and V.I. Zakharov, 1980, Phys. Rev. Lett. **45**, 688.

Wells, J.D. and G.L. Kane, 1996, Phys. Rev. Lett. **76**, 869.

Willenbrock, S.S.D. and D. Dicus, 1986, Phys. Rev. D **34**, 155.

Woods, M., 1996, in *Proceedings of the International Europhysics Conference on High-Energy Physics*, edited by J. Lemonne, C. Vander Velde, and F. Verbeure (World Scientific, Singapore), p. 31.

Yao, W., 1995, to be published in *Proceedings of the 17th International Symposium on Lepton-Photon Interactions*, Beijing, China.

Yoshida, H. *et al.*, 1987, Phys. Lett. B **198**, 570.

Yuan, C.P., 1990, Phys. Rev. D **41**, 42.